LUND UNIVERSITY
Faculty of Science

Electrical Properties of planar Metal-GdN-Metal junctions for Spintronic Applications

Felicia Ullstad

Thesis submitted for the degree of Master of Science
Project duration: 10 months

Supervised by Jonas Johansson, Lund University and
Franck Natali, Victoria University of Wellington

Department of Physics
Division of Solid State Physics
June 2015

Abstract

In this thesis the properties of planar metal-gadolinium nitride-metal junctions have been studied with the aim of establishing ohmic and Schottky contacts to thin polycrystalline films of n-type gadolinium nitride (GdN). GdN is an intrinsic ferromagnetic semiconductor of the rare earth nitride series. Samples and planar junction devices were grown on sapphire substrates, and the metal contacts were pre-deposited and not annealed. GdN films have been grown at room temperature in a ultra high vacuum system using the physical vapour deposition technique, using solid Gd targets and pure molecular nitrogen as a nitrogen precursor. Nitrogen partial pressures were kept around 10^{-5} mbar and deposition growth rates around 2 Å/s. The planar junction devices were tested at temperatures between 5 K and 300 K and the GdN films have resistivities between $3.7{\cdot}10^{-4}$ Ωcm and 1 Ωcm. Devices were made with contacts out of Au, Ag, Gd, Ti, and Ti/Al bilayer. The manufactured devices display ohmic and rectifying current-voltage characteristics depending on the metal used in making the device. The temperature dependent resistance of the devices show characteristic GdN behaviour.

As a metal-GdN-metal junction would be the building block of any REN-based spintronic device, the understanding of their electrical properties is of major importance. Therefore the electrical characterisation of this system is the main goal of this thesis.

The experimental work and analysis in this thesis was performed in the Spintronics group at the School of Chemical and Physical Sciences at Victoria University of Wellington.

Published peer reviewed material:
Felicia Ullstad, Jay R. Chan, Harry Warring, Natalie Plank, Ben Ruck, Joe Trodahl and Franck Natali
Ohmic contacts of Au and Ag to n-type GdN thin films
AIMS Material Science **2**(2): 79-85 (2015)

Further results to be published

Contents

1 List of Abbreviations and Acronyms

- RE - Rare Earth
- REN - Rare Earth Nitride
- GdN - Gadolinium Nitride
- GaN - Gallium Nitride
- NdN - Neodymium Nitride
- SmN - Samarium Nitride
- T_C - Curie Temperature
- SBH - Schottky Barrier Height
- MBE - Molecular Beam Epitaxy
- UHV - Ultra High Vacuum
- DMS - Dilute Magnetic Semiconductors
- PPMS - Physical Property Measurement System
- XRR - X-Ray Reflectivity
- XRD - X-ray Diffraction
- AFM - Atomic Force Microscopy

2 Introduction

The first papers on the rare earth nitrides were published in the 1960s, when it was finally possible to chemically separate the elements in the lanthanide series from each other. For a few years they were widely studied experimentally, but the low quality of the samples due to high densities of nitrogen vacancies and oxygen contamination put the interest in the materials on hold. Only a few papers were published from the 1980s to the 2000s. With the improvement in vacuum technique over the last two decades and theoretical advancements it is now possible to grow high quality thin films and compare their physical properties with theoretical predictions [1].

The rare earths comprise the elements from lanthanum to lutetium through which the 4f level is being filled. This means that they display the highest spin and orbital moments of all stable elements. The rare earths are found in many magnetic materials, sometimes as a main constituent but often as a dopant. They are for example used in alloys and heterostructures with other magnetic materials such as Co and Fe to adjust their magnetic properties [2–4].

The most studied compound of the rare earth nitrides is gadolinium nitride (GdN). GdN has an intricate conducting character. Predictions from band-structure calculations include semiconducting and half-metallic. Many research groups have worked with characterising GdN thin films grown under different conditions and it is now quite accepted that GdN is a ferromagnetic semiconductor. It has been studied in terms of temperature-dependent resistivity and photoconductivity, magnetic properties, transport properties and how it behaves under different forms of doping[5–9].

The rare earth nitrides are chemically and structurally similar, but show a wide range of properties useful in spintronic applications. Their electronic ground states range from semiconductors (GdN, DyN, ErN, SmN) to half-metals (EuN). They show ferromagnetic (SmN, GdN, TbN, DyN, HoN, ErN), antiferromagnetic (YbN), and paramagnetic (EuN) properties [1, 10].

Ferromagnetic semiconductors offer one great advantage over traditional metallic ferromagnets in spintronic applications in that they allow for total spin polarisation of the electrons which is necessary for highly efficient spintronic devices. It is very rare to find a material that is intrinsically semiconducting and ferromagnetic. Some of the currently known intrinsic ferromagnetic semiconductors are for example $CrBr_3$, EuO, $CuCr_2Te_3I$, DyF_3 and $EuLiH_3$. The rare earth nitrides offer an interesting complement to these materials in that they are chemically and structurally similar which allows them to be easily combined for tailored device manufacturing [1, 11].

There are already proof of concept GdN devices out there; a GdN-based spin filter Josephson junction [12, 13], GdN nano island based GaN tunnel junctions [14], spin-filtering nanocontacts [15], heterostructures with topological insulators [16], field effect transistors [6] as

well as GdN magnetic tunnel junctions [17]. These are of interest for the development of spintronic devices and quantum computation.

The aim of this thesis is to make devices to investigate how different metals work as contacts to GdN films of different resistivity to further the understanding for device manufacturing featuring GdN. The devices consist of a planar metal-GdN-metal junction and will serve as building blocks for further device manufacturing. Metals that have been tried as contacts in this work are gold (Au), silver (Ag), gadolinium (Gd), titanium (Ti), and Ti/Aluminum (Al) bilayer.

The thesis is comprised of six sections with this introduction being the first. Second is a theory section where the properties of GdN and GdN devices are discussed as well as the theoretical background to the growth process and resistivity measurements. Third is a method section where the growth process, device manufacturing and measurement techniques are described in detail. The following fourth section shows the experimental results. Fifth, a discussion about the results follows the results section. The thesis finishes with the sixth section, an outlook about the possible uses and further directions of this research.

3 Theory

In this section we will provide an introduction to spintronics, a theoretical overview of the properties of the rare earth nitrides, of GdN (e.g. magnetic and electrical), ohmic and Schottky contacts in general and for GdN specifically as well as the theoretical background for molecular beam epitaxy and van der Pauw resistivity measurements.

3.1 Introduction to Spintronics

Spintronics is a type of electronics based on the spin of the electron. The spintronic devices can either rely solely on the spin of the electron or use the spin in combination with the charge of the electron. Potential applications are found in spin-effect transistors, spin-logic devices and quantum computers [18–20].

Spintronic devices based on ferromagnetic metals have been around since the discovery of the giant magnetoresistance (GMR) in the 1980s, where the resistance of multilayers of ferromagnetic materials and nonmagnetic material is dependant on the orientation of the magnetisation of the adjacent ferromagnetic layers. Semiconductor-based spintronic devices are a bit more recent invention and offer hopes of integrating it more smoothly with existing electronics.

In a spintronics device one wants to obtain a non-equilibrium spin population. This can be done by optically exciting carriers with polarised light, or by injecting polarised carriers electrically. Traditionally the spin of the electron has been changed by passing it through a ferromagnetic material, allowing it to reorient in its magnetic field.

Dilute ferromagnetic semiconductors (DMS), which are formed by a dilute concentration of magnetic atoms incorporated into a semiconducting material, are seen as the most promising materials for spintronics device applications. To date the front runners are GaN and wide band gap materials doped with transition or rare-earth metals, based on the expectation of these devices operating above room temperature [3, 21]. However although there has been a lot of progress over the last decade to accomplish this task, there is still a lack of complete understanding of the ferromagnetic exchange interaction. Furthermore growth issues such as the segregation of secondary phases or generation of defects when increasing the dopant concentration must still be overcome [22, 23]. On top of that, in such systems the magnetic dopants also tend to act as electronic dopants making it difficult to control independently the carrier concentration and the magnetism [1, 24].

The remedy to this could potentially be found in intrinsic ferromagnetic semiconductors, something that the Rare Earth Nitride (REN) family is full of.

3.2 Rare Earth Nitrides

The rare earths contain the elements from La to Lu, as well as Sc and Y, through which the 4f level is being filled. The 4f electrons have a high angular momentum keeping them separated from other valence shells and the 4f wave function has no node. This leads to the 4f electrons being very localised and atomic-like in nature [1].

The rare earths are all trivalent (except Ce in CeN which is tetravalent [8, 25]) and three electrons contribute to the compound when bonding with nitrogen. All the RENs crystallise in the rocksalt crystal structure. As a result of the simple crystallographic structure in combination with their interesting electronic properties they have become model compounds for testing band structure calculations [1].

Due to the 4f-orbital filling up through out the lanthanide series the rare earth nitrides (RENs) have very interesting magnetic properties. Some are intrinsically ferromagnetic, some are antiferromagnetic, and some are paramagnetic. This trait coupled with most of the rare earth nitrides being semiconductors makes them a group of compounds that is worthy of intense research.

Since the rare earth nitrides are intrinsically ferromagnetic semiconductors, they allow doping independent of magnetism. This gives the RENs a huge advantage over DMS in spintronic applications. The RENs exhibit a spin splitting of a few hundred meV on both band edges, with the majority spin having a lower energy resulting in all carriers being in the majority bands [1, 26, 27].

3.3 Properties of GdN

In GdN the 4f orbital is half-filled leading to the spin magnetic moment being maximised and the orbital magnetic moment being zero. This gives a theoretical total magnetic moment of GdN of 7 μ_B/Gd [25]. It is also found experimentally to saturate at 7 μ_B/Gd [7].

GdN is the only element in the Gd-pnictides (compounds of Gd and elements from group 15 in the periodic table) that is ferromagnetic, the rest being anti-ferromagnetic [28–30]. However, GdN has been shown to display a dual-phase behaviour with competing ferromagnetic and antiferromagnetic order when grown with reactive magnetron sputtering thought to originate from the nitrogen vacancies in the films [30].

GdN grown under the same conditions as our samples show a ferromagnetic semiconducting ground state [5]. GdN has an indirect band gap of about 0.4 eV with the valence band maximum at X and the conduction band minimum at Γ[1]. GdN has an optical gap of 1.3 eV

[1] X and Γ are points of high symmetry in the reciprocal space of the crystal lattice.

at room temperature and 0.9 eV under T_C due to the spin-splitting of the bands [31]. The optical band gap is found to widen as GdN get thinner in some studies [32].

It has been suggested that the thickness of GdN is also important for determining the magnetic state it is in. For thin films of 16 nm GdN appear to be superparamagnetic but it is uniformly ferromagnetic for thicker films of 120 nm [33]. However there are also results published showing uniformly ferromagnetic GdN for a film thickness of 14 nm [7]. Another parameter affecting the properties of GdN is the strain during growth. GdN grown with an extended lattice parameter of 2.4 % has a reduced magnetisation and the Curie temperature is lowered from 69 K to 20 K [34].

The ferromagnetic behaviour of GdN has been described using the Ruderman-Kittel-Kasuya-Yosida (RKKY) model [29]. This model describes and calculates the exchange interaction between localised core spins mediated by metallic ion gas. This is used for metallic ferromagnets but with some modifications it is possible to use it for ferromagnetic semiconductors as well. The ferromagnetism in GdN has also been attributed to the superexchange interaction [32]. Using the RKKY model it is possible to predict the Curie temperature of GdN. The Curie temperature of GdN is theoretically predicted to be around 20 K in most calculations [35] and using a modified RKKY-like exchange interaction for carrier-mediated ferromagnetism T_C has been predicted to be peaking at 60 K at doping levels near 10^{20} cm^{-3} [36]. T_C is generally found experimentally between 30 K and 70 K depending on the experimental method and conditions [1, 5, 32, 34, 37]. This is thought to depend in part on nitrogen vacancies [26] but also the existence of magnetic polarons [6, 38]. The existence of polarons in GdN was strengthened by the findings that Mg-doped GdN has a lower Curie temperature [9].

The main dopant of the rare earth nitrides is nitrogen vacancies [26, 27]. The resistivity of thin films of GdN is mainly controlled by the amount of nitrogen vacancies in the film. Nitrogen vacancies are present in all grown samples and it is difficult to grow a GdN film with a nitrogen vacancy content under 1%. The vacancies supply the GdN film with up to 3 electrons per vacancy, leading to n-type GdN films. The nitrogen vacancies form a donor level about 20 meV below the conduction band. When growing the rare earth nitrides using molecular beam epitaxy (MBE) the doping level can be controlled by changing the nitrogen partial pressure in the UHV chamber during the growth. This allows all types of films from conductive to highly resistive to be grown. Studies monitoring the resistivity of a GdN thin film, during MBE growth, using predeposited Ag contacts have shown that changing the nitrogen growth pressure changes the resistivity of the GdN film [5]. Studies have also been done on GdN doped with the acceptor Mg [9]. These show a reduction in electron density and an increase in resistivity. The Curie temperature is also lowered as expected when the electron density is decreased.

The temperature dependent resistivity curve of GdN can be explained in terms of thermal excitations and spin splitting of the conduction band. The resistivity of GdN increases as the temperature decreases due to carriers being frozen out of the conduction band. When reaching

the Curie temperature, the ferromagnetic transition sets in. The resistivity decreases as the GdN goes through the ferromagnetic transition due to the spin splitting of the conduction band. The energy of the majority spin band is lower than that of the non-spin split conduction band energy level. This smaller energy gap allows more thermally activated electrons from the donor level to go into the conduction band. Since the majority spin energy level remains fixed relative to the conduction band energy level the resistivity starts to increase again as the temperature decreases further as the carriers that were excited into the conduction band are once again frozen out of the conduction band.

GdN is very sensitive to air, requiring it to be grown with a capping layer. Gd has a very high affinity for oxygen, leading to GdN decomposition and the formation of gadolinium oxide in less than a minute if left exposed to ambient conditions [39]. Our devices are therefore grown with a 50 nm GaN capping layer.

GdN grows epitaxially using MBE at temperatures ranging between 700 K and 850 K [1]. When growing GdN using solid Gd and N_2 as a nitrogen precursor it is not necessary to ionise the nitrogen as Gd acts as a catalyst for breaking the N_2 molecular bond [40].

3.4 Metal - Semiconductor junctions

When a metal is brought in contact with a semiconductor their Fermi levels[2] align. Depending on the initial position of the Fermi levels of the metal and semiconductor and energy of the valence and conduction band of the semiconductor there are two types of behaviour that can be observed for current transport. If the current-voltage (IV) characteristics are linear the contact is said to be ohmic. If the IV-characteristics are nonlinear the contact is said to be rectifying or Schottky type. In an ohmic contact there is no, or a very low, barrier to charge carriers to move between the metal and semiconductor. However in a rectifying contact the junction only conducts current in forward[3] bias, letting no or little current through in reverse[4] bias [41].

In a system where there are two metal contacts to the semiconductor through which the semiconductor is being electrically contacted, assuming the metal-semiconductor junction is rectifying, one of the junctions will always be under reverse bias and the system will be dominated by the behaviour of this junction. In our device setup we have a back-to-back diode system - the system will always be dominated by the reverse bias behaviour if the junction is rectifying [42].

If the electrical contact between two materials is ohmic or rectifying (Schottky) depends on

[2]The energy level of a body which at thermodynamic equilibrium has a 50% possibility of being occupied.
[3]The metal in the junction is connected to the positive terminal of a voltage source.
[4]The metal in the junction is connected to the negative terminal of a voltage source.

the Schottky barrier height (SBH). This is an electrical barrier between two materials due to their differing locations of the conduction band, valence band and Fermi level.

In figure 1 we see the band diagrams of a metal-semiconductor junction. Since GdN is n-type we will focus on junctions with n-type semiconductors.

First we need to introduce the concepts of work function and electron affinity. The work function (Φ) of a material is the energy needed to move an electron with the energy of the Fermi level to infinity. The electron affinity (χ) is the energy difference in a semiconductor between the bottom of the conduction band and infinity.

If the metal work function (Φ_M) is lower than the semiconductor work function (Φ_S), $\Phi_M < \Phi_S$, the result is an ohmic junction. When the metal and semiconductor are brought in contact electrons will flow from the metal to the semiconductor to lower their energy. This results in charging of the interface and deformation of the semiconductor bands. The energy band levels at the interface are pinned and does not move, but further from the interface the semiconductor bands are shifted upwards. This is called accumulation and can be seen in figure 1(a). In the ohmic junction the electrons are free to move between the metal and semiconductor. When a bias is applied to the ohmic junction it will not restrict the current flow in any way, making the current-voltage characteristics of an ohmic contact linear.

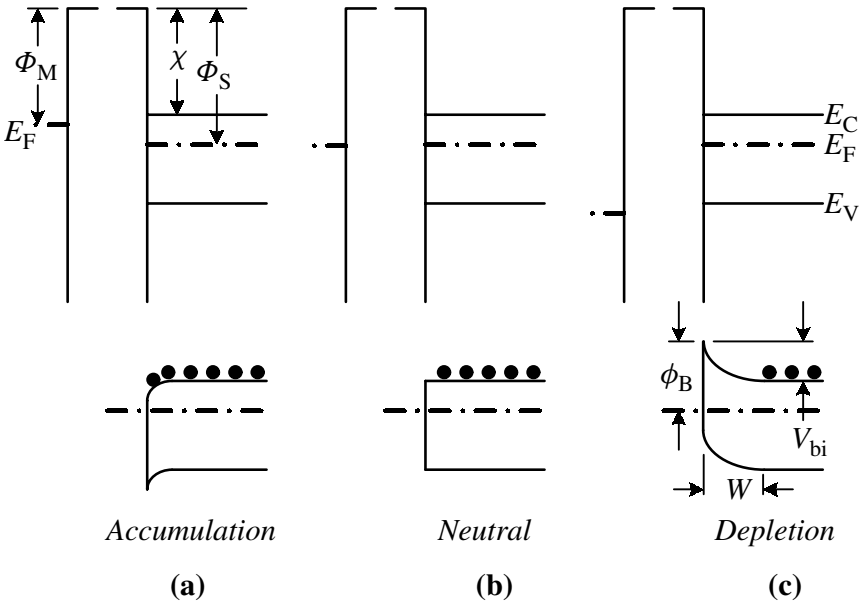

Figure 1: Schematic energy band diagrams of metal-semiconductor junctions in the case of a) Ohmic b) Neutral c) Schottky. From Ref. [41]. Used with permission.

If the metal work function is higher than the semiconductor work function, $\Phi_M > \Phi_S$, the result is a rectifying junction. This can be seen in figure 1(c). Upon contact between the

metal and semiconductor electrons flow from the semiconductor to the metal resulting in the semiconductor bands being deformed and shifted downwards due to the charging of the metal. This leads to the formation of a depletion zone where no electrons are residing, marked with W in figure 1(c).

When a forward bias is applied to the rectifying junction the apparent SBH is lowered by the bands shifting upwards from their non-biased state, leading to a shrinking of the depletion zone. This makes it easier for electrons to overcome the barrier. Electrons can either tunnel through the barrier or overcome it by thermal excitation, depending on the energy required.

When a reverse bias is applied to the rectifying junction the apparent SBH is increased by the bands shifting downwards from their non-biased state. The depletion zone grows, making it harder for electrons to overcome the barrier. This generally means that there is no current flowing in the reverse bias until such a point as the applied voltage is high enough to cause break-down of the junction.

To achieve an ohmic junction one should use metals with low work functions and to get a rectifying junction metals with high work functions should be used.

3.5 Contacts metals

When choosing metals for making contacts to semiconductors it is important to make sure they will not degrade over time and diminish the performance of the device. The noble metals popular for this purpose due to their high resistance to corrosion and oxidation. Titanium is also used due to it's high corrosion resistance. Since GdN is a n-type semiconductor it is interesting to study what kind of contacts are popular for other similar semiconductors.

As-deposited Au contacts on n-type GaN were found to be rectifying, but turning ohmic after annealing due to Au-in-diffusion. Al contacts to the same GaN were ohmic, both when as-deposited (no treatment after being deposited) and after annealing [43].

Ti/Al/Pt/Au and Ti/Al contacts have been found to produce very stable ohmic contacts to n-type GaN [44, 45]. Multilayer contacts Ti/Al/Ni/Au for n-GaN are ohmic when GaN has been prepared by reactive ion etching leaving a highly n-type GaN surface for the metal to contact [46].

Ohmic contacts have been made to InAlAs/InGaAs/InP transistors using Ag containing contacts. The ohmic behaviour is suggested to depend on Ag in-diffusion into the transistor material [47].

Silver-antimony contacts(99%-1%) have been used for n-type Ge. It was suggested that the ohmic contact formed was due to increased doping at the interface due to preferential Sb evaporation [48].

Gd has been tused as a spin tunnel contact for silicon [49], but more importantly GdN consists of 50% Gd making Gd interesting for device contacts as it is easily available during device manufacturing. Gd also has a very low work function, see Table 1, which is desirable for making ohmic junctions.

With these references in mind we choose to study the electrical behaviour of contacts containing Au, Ag, Ti, Al, and Gd in junctions with GdN. See Table 1 for a list of the work functions of the used metals. When depositing Ag and Au, a thin layer of Cr is deposited first as Ag and Au does not stick very well to sapphire. Cr is not used on its own in any contacts.

Table 1: Metals used in contacts and their work functions. From Refs. [50, 51].

Metal	**Work function** (eV)
Cr	4.5
Au	5.1-5.47
Ag	4.0-5.02
Ti	4.33
Al	4.54
Gd	3.1

3.6 Molecular Beam Epitaxy

Molecular Beam Epitaxy (MBE) is a ultra high vacuum based technique where directed beams of vapour of atoms or molecules form ordered epitaxial layers on a substrate. A MBE system consists of a vacuum chamber made of stainless steel or aluminium alloys. It contains high purity source materials, either in solid, liquid, or gas phase. There are shutters for accurately controlling the thickness and composition of the grown material. Included in the MBE system is also substrate manipulation arrangements, and diagnostic and analytical facilities [52, 53].

The chamber pressure is kept very low, at pressures around 10^{-9} mbar, to reduce the amount of impurities in the films grown [52, 53]. This is especially important when growing with highly reactive species such as Gd, which acts as a getter [5].

When growing a film it is usually rotated to give an even distribution of particles on the substrate. The deposition rate is typically around 1 monolayer/second. The temperature of the substrate is often around 1000 K to promote epitaxial growth [52, 53].

The films grown for this thesis have all been grown inside a MBE system using electron beam physical vapour deposition.

3.7 Four point probe (van der Pauw) resistivity measurements

A common way of measuring resistivity of semiconductors is by the four point probe technique, also known as the van der Pauw technique. Four probes are set up either in a line or in a square arrangement, as in figure 2. Current is passed between two adjacent probes and the voltage drop is measured between the two remaining probes.

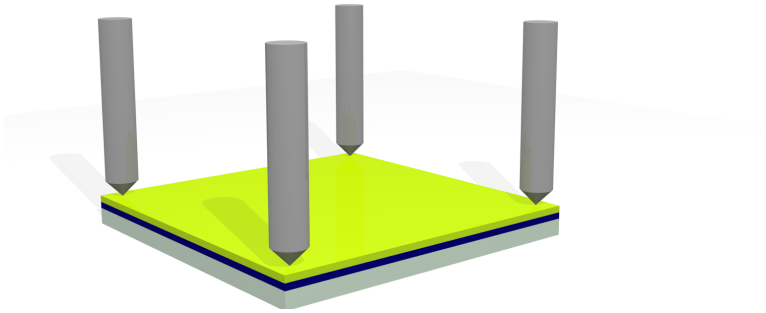

Figure 2: Four point square probe array

For a thin sample the resistivity can be found as

$$\rho = \frac{\pi}{\ln 2} \cdot \frac{V}{I} \cdot t \tag{1}$$

where V is the voltage, I the current and t is the thickness of the sample. The correction factor $\frac{\pi}{\ln 2}$ has been calculated using geometrical considerations and assuming that the probes are arranged square in the corners of the sample and also assuming that the probe contact to the sample can be approximated as a point contact. [54–57]

The advantage of doing a four point measurement, instead of the common two point, is that the resistance contributed from the electrical contacts can be removed, as opposed to when doing a two point measurement when the contacts can contribute heavily to the total resistance of a sample. Once the contact resistance has been removed it is possible to calculate the resistivity of the sample. The resistivity measurements in this thesis have been made using the square four point probe array. Device resistance measurements have been done using both the square four point probe array and the common two point measurement depending on the device structure.

4 Method

4.1 Making the devices

4.1.1 Contact deposition

All devices have been made with polycrystalline GdN on predeposited contacts on a blank sapphire substrate. The GdN was capped with GaN to prevent it from oxidising. Contacts were deposited onto the sapphire in different ways, depending on the desired contact geometry and contact metal.

Device structure I: The first samples were made by evaporating metals through a thin gold shadow mask onto the sapphire substrates in a Angstrom Engineering NEX DEP 200 Evaporator. The shadow mask was constructed to make six pairs of metal contacts on every piece of sapphire (15 mm $\times$ 20 mm). The six contact pairs had contact separations of 30 μm, 40 μm, 50 μm, 60 μm, 80 μm and 100 μm (see figure 3 for a schematic of the growth geometry). The sapphire pieces were fixed in place under the shadow mask by carbon tape and after metal deposition the devices were sonicated in acetone to remove all carbon tape residues.

Using deposition through a shadow mask does unfortunately not allow the mounting plate with the sapphire substrates to rotate during metal evaporation as this causes metal influx where there is supposed to be a gap between the two metal pads of each device. This means that the metal contacts will be slightly uneven in thickness as the flux impinging on the substrate through the shadow mask is not the same everywhere.

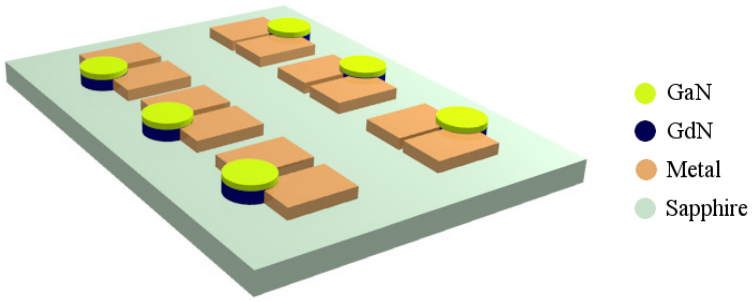

Figure 3: Schematic of one set of six devices made with shadow masks

Using the evaporator also limits what metals can be used for contacts as the pressure only goes down to a lowest of 10^{-7} Torr during a typical evaporation run and the highest pressure to operate is 10^{-5} Torr. This means that it is only possible to use metal targets that will not outgas too much relative to the metal evaporated. This ruled out using gadolinium for use in the evaporator leading to a second device structure being designed. Devices with contacts

made out of Au, Ag, Ti and Ti/Al were made using shadow masks. This device design allows for 2-point IV-measurements to its two metal contact pads or quasi-4-point van der Pauw measurements, as when four contacts are made to the device they are essentially pair-wise short circuited through the metal contact giving the result of a two point measurement. These shortcomings lead to the design of device structure II where there are four predeposited metal contacts instead.

Device structure II: The second way that contacts were made was using photolithography. A 10 mm $\times$ 10 mm blank piece of sapphire was put into a spin-coater. AZ1518 photoresist was dripped onto the sapphire and the spin-coater was then run for 60 seconds at 4000 rpm. The photoresist-covered sapphire was put into a Karl Suss MJB3 Mask Aligner under a photomask. The photomask was designed in the program LayoutEditor and made using Electron Beam Lithography by Canterbury University. The geometry of the finished device can be seen in figure 4. This device design allows for four-point measurements across well defined gaps of either 30 μm, 50 μm, or 100 μm.

After putting the photoresist-covered sapphire into the mask aligner it was exposed with UV-radiation for 13 seconds. It was stirred around in developer for 35 seconds and then rinsed with deionised water. The resulting pattern was studied under a microscope to assess the quality. The patterned sapphire was then exposed to the desired contact metals, either Au in the Angstrom Engineering evaporator or Gd in a Thermionics UHV system using the e-gun inside to evaporate the Gd metal. After depositing the desired metal, the metal-covered sapphire was left to sonicate in acetone for 30 minutes to remove all the metal outside of the lithography pattern, leaving behind the 4 metal contact pads. This device structure allows for 2-point IV-measurements as well as 4-point measurements since it is possible to choose which metal contact pads are used in each experiment.

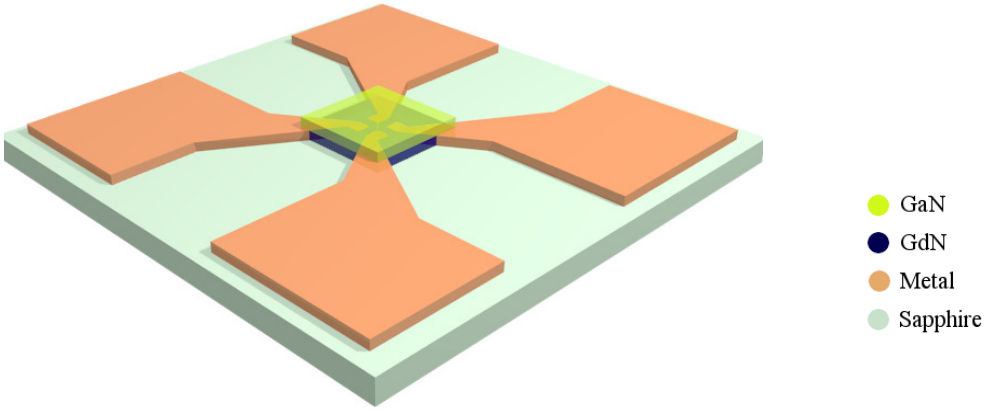

Figure 4: Schematic of a device made using photolithography. GaN and GdN have been made transparent in the sketch to show the metal structure underneath.

Devices with contacts made of Gd were made in this structure using an electron gun inside a Thermionics UHV system. The electron gun was used to heat up a crucible with solid Gd metal to allow it to evaporate onto the photolithography-patterned sapphire. Some Au devices were also made using this structure in the Angstrom Engineering NEX DEP 200 Evaporator.

All contacts were 50 nm thick in total (except the Au and Ag that also had a 3 nm layer of Cr between them and the sapphire to make the metal stick properly to the sapphire) and the metal deposition rate was kept below 1 Å/s. The Ti/Al contacts were made with 15 nm Ti and then 35 nm Al on top.

4.1.2 Growing GdN on pre-deposited contacts

Devices were made in six different batches where the growth conditions were controlled so that the deposited GdN in the different batches had different resistivities. Each batch included a bare sapphire substrate, a bare silicon substrate and a number of sapphire substrates with pre-deposited metal contacts, either with device structure I or II. The bare sapphire was used to be able to characterise the GdN film that was used in all the devices in the same batch without having to take the metal and structure of the device into consideration as well. The bare silicon substrates were used to be able to characterise the GdN and GaN layer thicknesses in a SEM, however this was unsuccessful. By studying the GdN films separate from the device geometry, on the bare sapphire substrates, it is easier to separate the effects due to the GdN in the device from the effects due to the metal and device design.

The sapphire substrate with the pre-deposited contacts was attached with kapton tape to a 2 inch diameter circular substrate holder. For device structure I a shadow mask with six round holes was used to only grow GdN on part of the device, particularly in the gap, leaving most of the contact pads free for direct electrical access. For device structure II a second layer of photoresist was applied and a second photolithography pattern was exposed on top of the 4-point geometry. See figures 3 and 4 for schematics of the devices. The contacts were not thermally annealed or sputtered before GdN deposition.

GdN was grown on top of the whole geometry and GaN was grown on top as a passivation layer to prevent the GdN from oxidising.

The GdN was grown in a Thermionics UHV chamber using physical vapour deposition. The vacuum was maintained using a backing pump and a turbo pump. A solid Gd target (purity: 99.9 %) in a crucible was heated up to above the melting point of Gd (1586 K) using an electron beam. The temperature of the Gd target was controlled by the intensity of the electron beam. The rate of evaporation was measured using a crystal deposition rate controller. When the Gd was evaporating at a rate of about 2 Å/s. N_2 (purity: 99.999 %) was introduced using a mass flow controller. The N_2 flux was increased until a total pressure of 2-8$\cdot 10^{-5}$ mbar was reached in the chamber. Growing in a lower nitrogen pressure gives a less resistive GdN film

due to nitrogen vacancies in the film acting as dopants. Typical thickness of the grown GdN films were around 100nm. The deposition rate was kept around 2 Å/s.

The GdN layer was capped with a layer of GaN, typically 50nm thick. The GaN was grown by heating up a solid Ga target in a crucible with an electron gun. N_2 was pumped in to the chamber at a rate of 10 sccm, leading to about $2.5{\cdot}10^{-4}$ mbar of N_2 in the UHV chamber. The nitrogen gas was ionised using a heated filament to allow it to react with the Ga and form GaN. The deposition rate was kept around 0.4 Å/s.

4.2 Characterisation of GdN films and devices

When the GdN films and devices from a batch were taken out of the UHV system they were immediately studied under an optical microscope to make sure that the gaps had the intended width and that the deposited GdN was free of major defects. They were then put into an Agilent 4156C Precision Semiconductor Parameter Analyzer for a quick room temperature IV-characterisation. Devices of particular interest were then put into a cryostat in van der Pauw geometry and temperature dependent resistance and IV-characteristics were measured at various temperatures down to 5 K. All GdN samples were studied by measuring the temperature dependent resistivity in a van der Pauw geometry in a cryostat to make sure they showed the expected behaviour of a polycrystalline GdN film. The GdN films were also studied using X-ray diffraction (XRD) to assess the crystalline quality, X-ray reflectivity (XRR) to measure the thickness of the GdN and GaN layers and using the Physical Property Measurement System (PPMS) to measure the carrier concentration. Some devices were studied using an atomic force microscope (AFM) to characterise the different device step interfaces.

4.2.1 Room temperature IV-characteristics

To perform room temperature current-voltage (IV) characteristics an Agilent 4156C Precision Semiconductor Parameter Analyzer was used. Two thin gold probe wires were places on two metal contact pads of the device. By looking through a microscope the gold probes were adjusted to make sure they were in contact with the device metal contacts. The gold probes connected the GdN device to a voltage source and ampere meter in the Parameter Analyzer. A voltage range was set by the operator and scanned through by the machine. The voltage and corresponding current were extracted from the Parameter Analyzer to a computer using a python script. The IV-characteristics were studied and the resistance from this two point measurement was calculated.

4.2.2 Temperature dependent carrier concentration

To measure the carrier concentration of the GdN films they were put into a Quantum Design EverCool Physical Property Measurement System (PPMS) located at Callaghan Innovation-Robinson Research Institute. A magnetic field of varying strength up to 9 Tesla was applied for two orientations of the sample (0° and 180°) at different temperatures. The Hall voltage across the film was measured. The difference between the two orientations was calculated and the slope for high magnetic fields was extracted manually. The carrier concentration of the film is proportional to the slope of the Hall voltage versus magnetic field in the linear region. The anomalous Hall effect was not considered when analysing the data as its contribution to the results was quite small.

4.2.3 Temperature dependent resistance, resistivity, and IV-characteristics

A Janis Research cryostat was equipped with a van der Pauw measurement setup. This allowed the temperature dependent resistance and resistivity of devices and GdN films to be measured in a four-point setup, see figure 5 for a schematic of the setup. A LabView program was used to control the cryostat and van der Pauw setup. Samples were put onto a removable copper block, with a thin layer of vacuum grease between the copper block and sample to increase the thermal conductivity. Sapphire is an insulator, removing the need to electrically insulate the sample from the copper block. The copper block was heated and cooled using an electrical heater and a helium compressor, allowing the copper block and the sample mounted on top of it to achieve temperatures between 4 K and 300 K.

Electrical contact to the sample was made by copper clips with soldered indium tips attached. The indium tips were pressed down on top of the sample, by screwing nylon screws down into the bottom copper block, to make good mechanical and electrical contact. The indium tips were reshaped using a soldering iron between every measurement to assure that they were a good approximation of point contacts and giving a mechanically strong contact to the sample. For some samples a small amount of silver paint was put between the indium tip and the sample to further increase the electrical contact. The indium tips, both with and without silver paint, give an ohmic contact to the GdN films and devices.

Copper wires were soldered onto the copper clips holding the sample down, and these wires were then soldered onto the electrical contacts in the cryostat used to pass current and measure the voltage drop across the sample.

A fixed current was passed through the film and the voltage was measured for different temperatures. The temperature change rate was set to 0.8 K/min, and data was collected while cooling the sample from 300 K to 5 K and also while heating it back up to 300 K to ensure that there was no temperature lag in the system. The setup was cooled using a helium compressor and the pressure was kept around 10^{-5} mbar. When running a resistivity as a function of temperature scan the current was fixed, usually at 10^{-4} A, and the changing voltage as the temperature changed was measured. When doing IV-characteristics of a device the voltage was measured at ∼40 different currents between 10^{-7} A and 10^{-2} A at 290 K, 200 K, 100 K, 60 K, 50 K, 40 K, and 5 K to see if the temperature or ferromagnetic transition changed the electrical behaviour of the device.

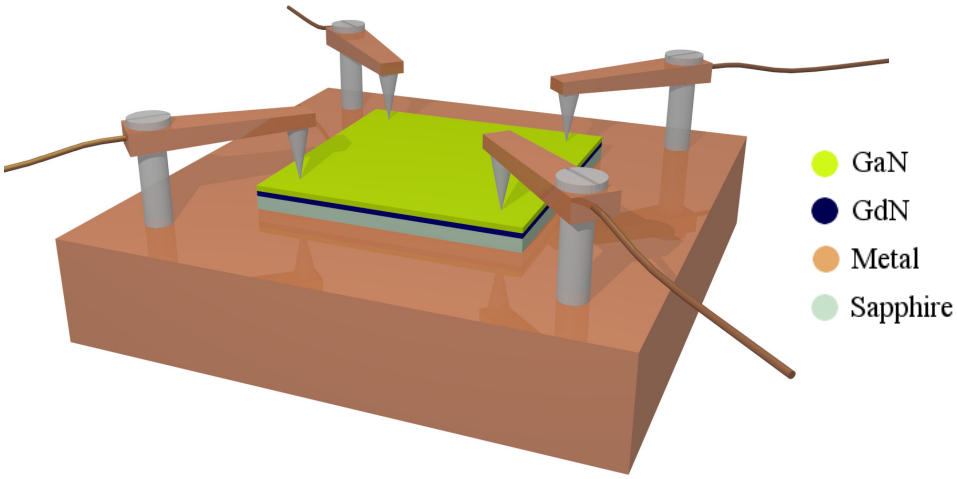

Figure 5: Schematic of cryostat setup. Copper block with the sample on. Sample is contacted electrically using copper clips with indium tips that are attached to the copper block using nylon screws.

4.2.4 Microscopy methods

The atomic force microscope (AFM) is a technique where a cantilever with a very sharp tip, ideally one atom wide, is placed close to a surface. The forces between the tip and the surface are measured by measuring the deflection of the cantilever. This allows the surface to be mapped in different ways depending on what resolution and type of AFM is used.

In this thesis an AFM was used to characterise the step profiles of the devices; the substrate-metal step boundary, the metal-GdN step boundary and the substrate-GdN step boundary. The surface roughness of the GaN capping layer was also measured. The experiments were done using a Nanosurf NaioAFM system and the data obtained was processed using the software Scanning Probe Image Processor (SPIP) 6.3.4.

5 Results

The result section is divided into a subsection for GdN thin films without metal contacts and subsections fot the different metals used to make devices. Gold and silver contacts work well as ohmic contacts to GdN while contacts made of gadolinium and titanium/aluminium bilayers are rectifying and titanium contacts lead to oxidisation and subsequent decomposition of the GdN.

Six different GdN depositions were made with varying resistivities, named A-F. The devices made with these GdN films with different metals are named e.g. Device A - Au - 40 μm whereas the bare GdN film grown at the same time in the same batch is named Sample A. All the different sample and device combinations are listed in Table 2. It lists the sample name, the nitrogen partial pressure used to grow that film and the resistivity achieved as well as the type of metals used with which device structure was made with that film.

The typical carrier concentration of the GdN films in this thesis were found to be around 10^{21} cm^{-3} when measured in the PPMS.

Table 2: GdN film and device data. The I/II in the metal column refers to what device design was used for that particular device. The film resistivities are given for 290 K.

Name	**N_2 growth pressure**	**Film resistivity**	**Metal**
A	$3.2{\cdot}10^{-5}$ mbar	$4.5{\cdot}10^{-4}$ Ωcm	Au (I)
B	$2.8{\cdot}10^{-5}$ mbar	0.017 Ωcm	Au (I)
			Ag (I)
			Ti/Al (I)
C	$2.4{\cdot}10^{-5}$ mbar	0.031 Ωcm	Au (I)
			Ag (I)
			Ti/Al (I)
D	$3{\cdot}10^{-5}$ mbar	0.13 Ωcm	Au (I)
			Ag (I)
			Ti/Al (I)
E	$8{\cdot}10^{-5}$ mbar	0.6 Ωcm	Au (II)
			Ag (I)
			Gd (II)
F	$5{\cdot}10^{-5}$ mbar	1.0 Ωcm	Au (II)
			Ag (I)
			Gd (II)

Table 2 will be useful for referencing back to while studying the rest of the Result section.

5.1 GdN films

In this section results are presented for samples that consist of thin films of GdN with no metal contacts are presented. The temperature dependent resistivity is presented as well as the resistivity's dependence on the nitrogen pressure during GdN deposition. All GdN films were studied using XRD and displayed preferential growth in the (111) direction as expected. XRR studies confirmed the thicknesses of the GdN and GaN layers as 100 nm and 50 nm respectively.

5.1.1 Temperature dependent resistivity

All measurements were performed using the van der Pauw setup in the cryostat. The typical temperature dependent resistivity of a GdN thin film can be seen in figure 6 where Sample C is shown. The resistivity was measured for GdN both while cooling the sample to 5 K and while heating it back up to room temperature to ensure that the temperature lag in the system is not affecting the results.

A peak in the resistivity can be seen around 50 K. This is located around the Curie temperature, the onset of ferromagnetic ordering in the GdN film. To determine the exact location of T_C one would have to do magnetic measurements as well, but it is well accepted that the peak in resistivity corresponds to the ferromagnetic ordering [1].

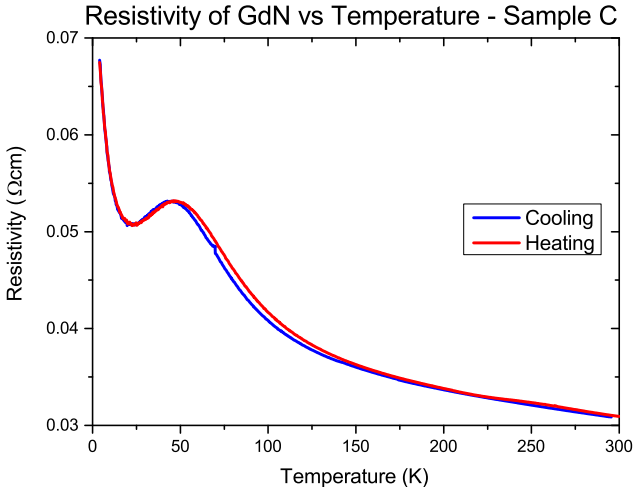

Figure 6: Resistivity versus temperature for sample C. The resistivity has been measured both when cooling and heating the sample.

As explained in section 3.3 the peak at T_C originates from the the splitting of the conduction band occurring as the GdN becomes ferromagnetic. The majority spin band is lower in energy then the non-split band energy level, allowing more thermally excited electrons into the conduction band as the ferromagnetic transition progresses which lowers the resistivity of the GdN. Once the ferromagnetic transition is complete the energies of the bands are fixed again leading to a freezing out of the electrons in the conduction band and an increase in resistivity as the temperature is lowered more.

The resistivity of the GdN films is changed by controlling the amount of nitrogen vacancies which is done by changing the nitrogen pressure in the UHV system. As the nitrogen pressure increases, the number of nitrogen vacancies decreases and the resistivity increases. In figure 7 we see the temperature-dependent resistivity for a few different samples with widely varying resistivities.

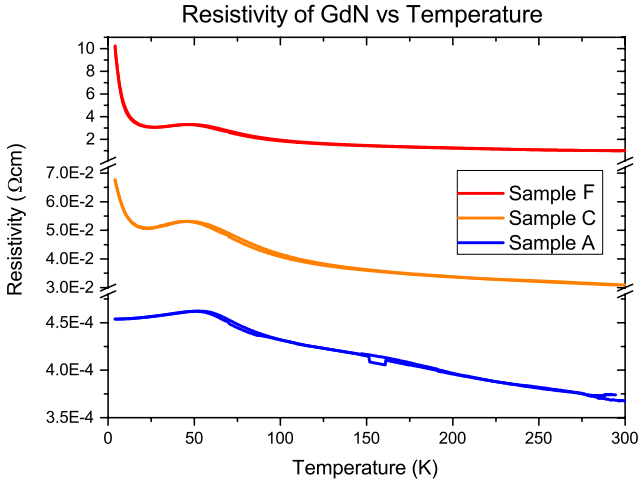

Figure 7: The temperature dependent resistivity for three different GdN films showing the range of resistivities used for this thesis.

In figure 8 we see the temperature-dependent resistivity for a few different nitrogen pressures. The diverging resistivity as T$\rightarrow$ 0 in combination with the resistivity being determined by the doping level confirms the idea of GdN as a semiconductor.

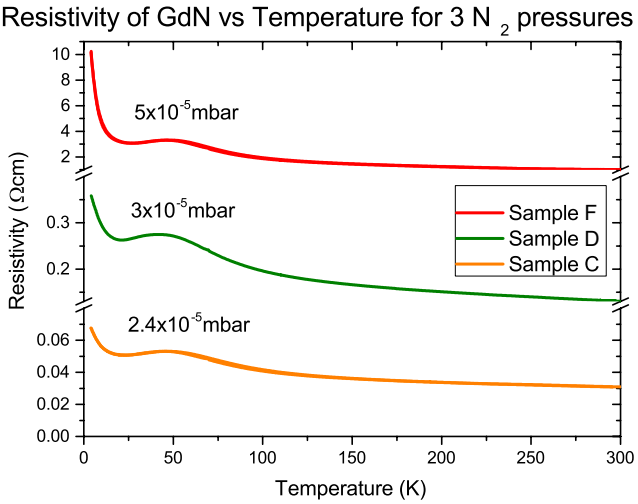

Figure 8: The temperature dependent resistivity for GdN films grown with three different pressures stated in the graph.

While the samples in figure 7 and figure 8 show the general trend of increasing resistivity as the N_2 pressure goes up, it is hard to draw any general conclusions about the resistivity's dependence on N_2 pressure from the samples grown. This is due to the crystal deposition rate controller not being accurate enough to allow the operator to keep a steady growth rate. This means that the Gd flux can change quite a lot before the change is seen on the deposition rate controller. Despite aiming to keep the N_2 pressure constant the changes in the Gd flux will change the composition of the GdN film and as a consequence also change the resistivity quite drastically.

5.2 Device structure

In this section all data relevant to device structure are presented. There are optical microscope images and AFM images and line scans.

5.2.1 Optical microscope images

Optical microscope images of the junction areas of two different device designs can be seen in figures 9 and 10.

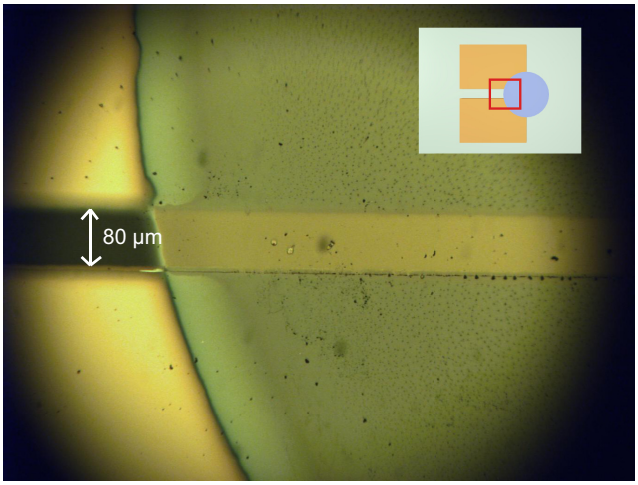

Figure 9: Device design I with a contact separation of 80 µm.

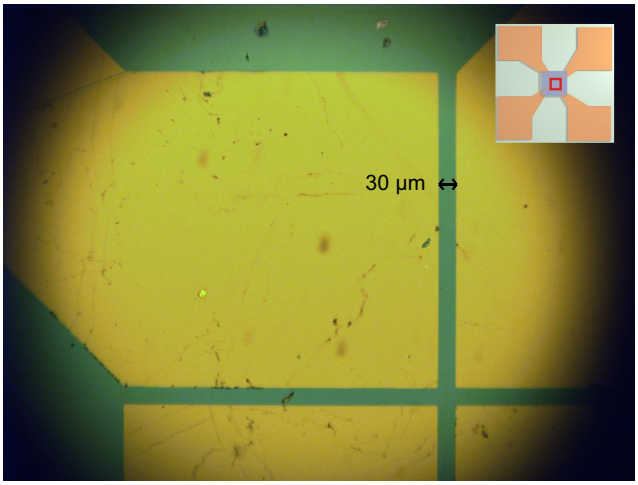

Figure 10: Device design II with a contact separation of 30 µm.

Inserts of figures 12 and 13: Red box outlines the area of the device displayed in the image.

Shadow masks for making metal contacts in device design I had the problem of metal vapour getting in under the shadowed areas which often lead to short-circuiting of the contacts making the deposited metal contact pair unable to be used for a device.

5.2.2 Atomic force microscopy results

When doing AFM on some of the manufactured devices it was concluded that most devices had well defined sharp edges, both devices using device design I and II. The only exception was a Ti/Al device in which the metal contact edges were gently sloping as opposed to the sharp edges of the other devices. This device can be seen in figure 11 for a 3-dimensional view of the sapphire-metal boundary and in figure 13 for line scans over both the sapphire-metal boundary as well as the metal-GdN boundary. This means that more of the underlying layer than intended will be in contact with the GdN. More metal overall will be in contact with the GdN which makes it possible to have more surface states at the interface which will influence the electrical characteristics of the device.

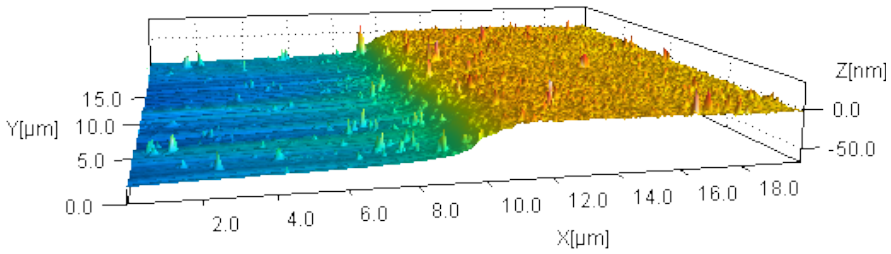

Figure 11: Device B - Ti/Al - 40 µm. Step from sapphire (top terrace) to Ti/Al contact (bottom terrace).

In figure 12 we see a 3-dimensional image of the sapphire-metal boundary of Device F - Gd - 50 μm. It has a very sharp boundary from being made using photolithography in device design II. Au devices made using device design I also have sharp boundaries. The sloped boundary of the Ti/Al contacts is thought to be caused by the bilayer structure, where the two metal layers might not have been deposited exactly on top of each other, which is why this is the only device showing this gradual step.

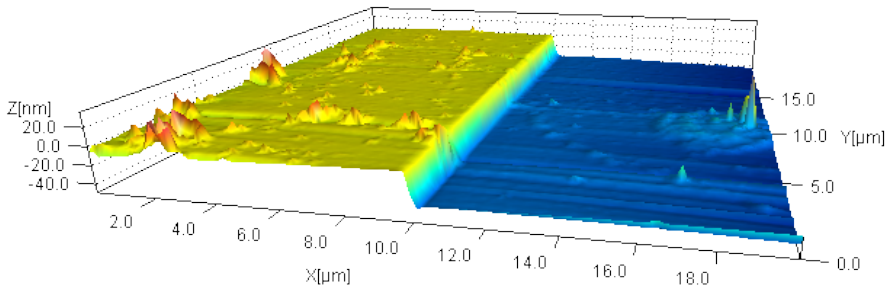

Figure 12: Device F - Gd - 50 µm. Step from Gd contact (top terrace) to sapphire substrate (bottom terrace).

In figures 13 and 14 some boundary line scans can be seen for the two previously shown devices. In figure 13 we once again see the sloped character of the Ti/Al device interfaces. The black curve shows the line scan from the sapphire substrate up onto the Ti/Al contact surface. The red curve shows the scan from the GdN on top of the contact down into the contact gap where there is only GdN. It shows the same sloped character as the scan over the bare contact edge but a bit more uneven due to the GdN and GaN films on top. It is also a slightly more curved interface than the sapphire-contact interface due to the semiconductor films growing over the junction and smoothing the boundary.

In figure 14 we see line scans of Device F - Gd - 50 μm. Due to its design using photolithography all boundaries are very sharp. The black curve shows the boundary step between the sapphire and the Gd contact. The blue curve shows the boundary step from the sapphire substrate to the GdN film. The peak at the top of the step in the blue curve is probably an artefact from the AFM tip overcompensating when reaching the high step. The red curve shows the boundary step from the GdN on top the Gd contact down into the gap between the the contacts. From these curves it is clear that all the boundary steps are very sharp. On the blue and red curves the surface roughness of the GdN and GaN layer can be seen.

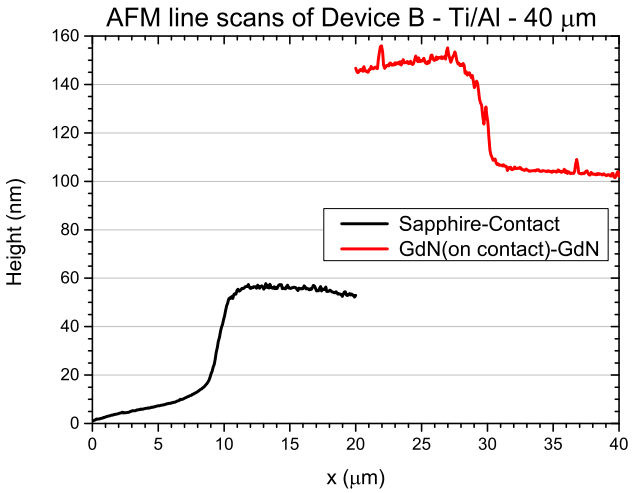

Figure 13: AFM line scans of Device B - Ti/Al - 40 μm.

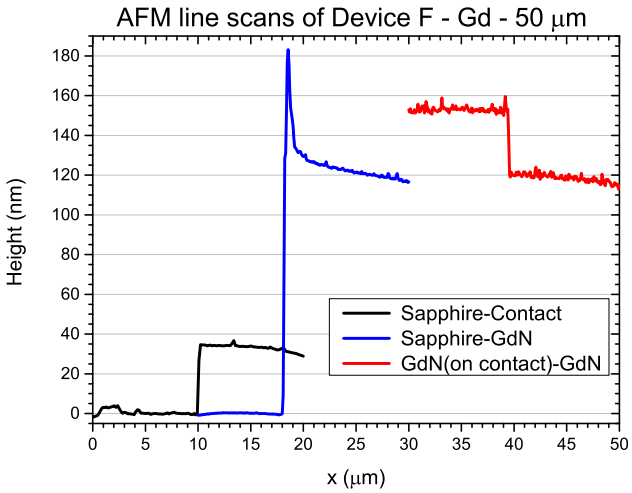

Figure 14: AFM line scans of Device F - Gd - 50 μm.

Legend states which boundary step has been scanned.

AFM measurements were also done on the GdN covered with GaN in the gap between the metal contacts to find out the surface roughness. This gives the surface roughness of the capping layer. The surface roughness was found to be 1.5 nm for the GaN capping layer during a 10 μm $\times$ 10 μm scan in the gap between the metal contacts of Device F - Gd - 50 μm.

5.3 Gold contact devices

Devices with gold contacts were made with GdN resistivities ranging between $4.5{\cdot}10^{-4}$ Ωcm and 1 Ωcm. The devices were made with a contact separation between 30 and 100 μm. Au devices were made using both device design I and II. All device separations with all the different resistivities of GdN at all temperatures between 5 K and 300 K displayed ohmic behaviour.

All Au contacts were 50 nm thick, with a 3 nm Cr layer underneath as Au does not stick very well to sapphire.

In figure 15 we see the temperature dependent resistance of a Device C - Au - 40 μm. This device is made with a GdN film resistivity in the middle range of resistivities used in this thesis.

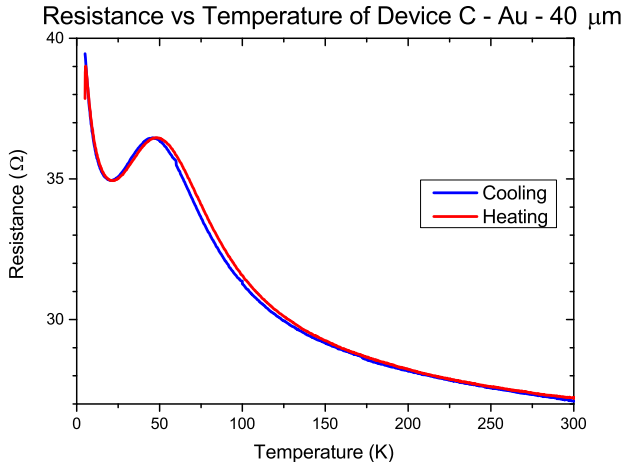

Figure 15: Resistance versus temperature for Device C - Au with 40 μm contact separation.

The temperature dependent resistance graph for the medium resistive Au device looks almost identical in shape to its film counterpart, see figure 7. Since this device in made with only two contacts it is not possible to compare it directly to the bare GdN film as a two contact device cannot be measured in 4-point van der Pauw geometry. It can only be measured using a quasi-4-point setup because two out of the four contacts have to be placed on each metal contact pad and these will be short-circuited essentially leading to a 2-point measurement.

In figure 16 we see the temperature dependent resistivity of Device F - Au - 30 μm and of Sample F. Since this device is made using device design II it can be directly compared to the GdN film resistivity from the van der Pauw measurements using equation 1. As we can see in figure 16 the resistivity of the Au device is not very different from the resistivity of the bare GdN film grown at the same time, indicating a very well functioning device without much effect from the GdN-metal interface.

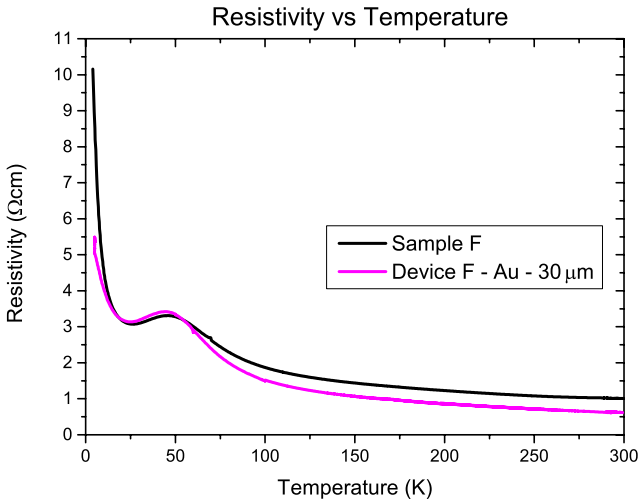

Figure 16: Resistivity versus temperature for Device F - Au with 30 µm contact separation compared with Sample F.

The IV characteristic of Device C - Au - 40 μm at 4 temperatures are shown in figure 17. The device shows ohmic behaviour at all temperatures between 5 K and 300 K. All other Au devices have shown ohmic behaviour as well, irrespective of GdN resistivity and contact separation. In figure 18 the IV-characteristics of the most resistive Au device is shown - Device F - Au - 30 μm. This shows that even the most resistive GdN film grown for this thesis gives an ohmic device when paired with Au contacts.

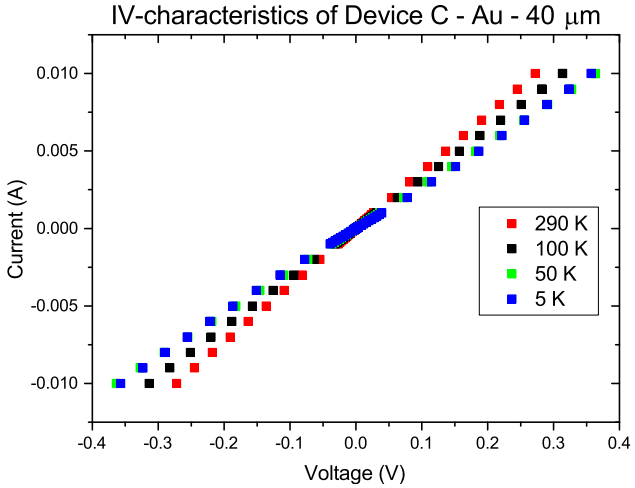

Figure 17: IV-characteristics of Device C - Au - 40 µm at 4 different temperatures.

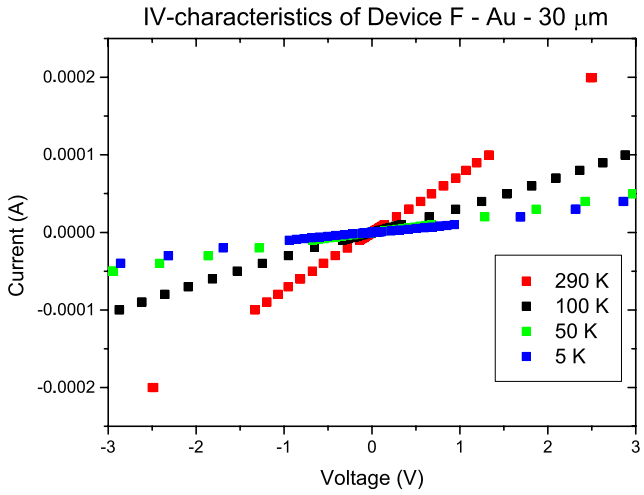

Figure 18: IV-characteristics of Device F - Au - 30 μm at 4 different temperatures.

5.4 Silver contact devices

The Ag contacts were 50 nm thick with a 3 nm adhesion layer of Cr as Ag does not stick very well to sapphire. Devices with Ag contacts were made with GdN resistivities between $1.7{\cdot}10^{-2}$ Ωcm and 1 Ωcm. All Ag devices were made using device design I.

In figure 19 we see the temperature dependent resistance of Device C - Ag - 80 μm. The device shows the same behaviour as a bare GdN film.

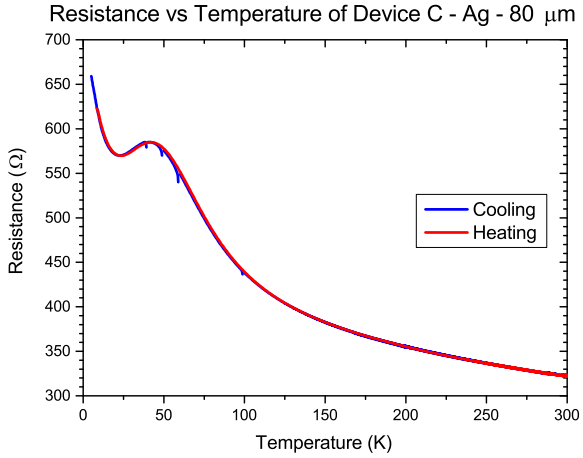

Figure 19: Resistance versus temperature for Device C - Ag - 80 μm.

In figure 20 we see the IV-characteristics of the device shown in figure 19. This and all other devices made with Ag contacts appear to have linear IV-characteristics at all temperatures between 5 K and 300 K and are therefore considered ohmic.

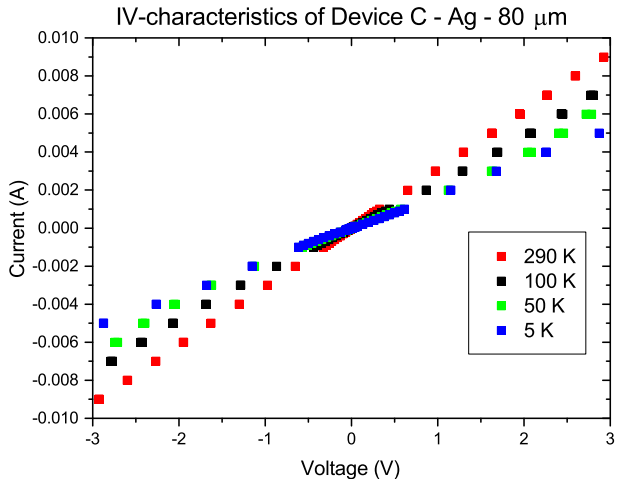

Figure 20: IV-characteristics of Device C - Ag - 80 μm at 4 different temperatures.

In figure 21 we see the temperature dependent resistance of a very resistive Ag device - Device F - Ag - 40 μm. There is just a slight shoulder in the resistance around 40 K suggesting a contribution from GdN. The lack of a clear peak could be from the device being quite old when this measurement was taken so it could have oxidised slightly. This suspicion is strengthened by measurements of Device F - Ag - 80 μm also just showing a very slight shoulder in the temperature dependent resistance. In figure 22 we see the IV curves for the same device at three different temperatures. They are all linear, suggesting ohmic junctions even for a possibly slightly oxidised Ag device.

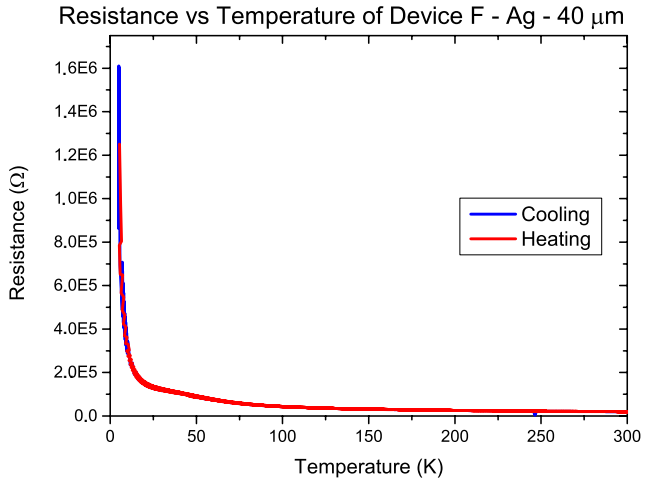

Figure 21: Resistance versus temperature for Device F - Ag - 40 μm.

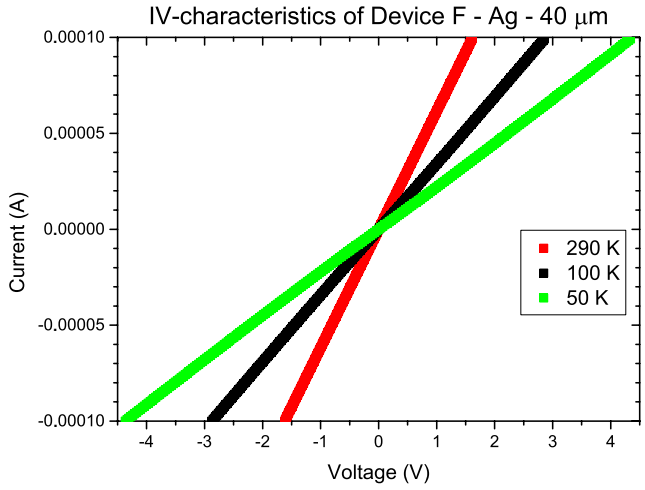

Figure 22: IV-characteristics of Device F - Ag - 40 μm at 3 different temperatures. At 5 K the voltage was too high for the voltmeter to measure.

5.5 Gadolinium contact devices

The Gd contact were around 50 nm thick. Device with Gd contacts were made with GdN resistivities ranging from 0.6 to 1 Ωcm. All Gd devices were made using device design II and the contact separations were 30 μm and 50 μm.

Figure 23 shows room temperature IV-characteristics of Gd contact devices with 2 different resistivities and two different contact separations. They are all clearly rectifying at room temperature. The measurements display the IV-characteristics of a typical back-to-back diode system where the IV-characteristics are non-linear close to zero but become linear as the voltage is increased.

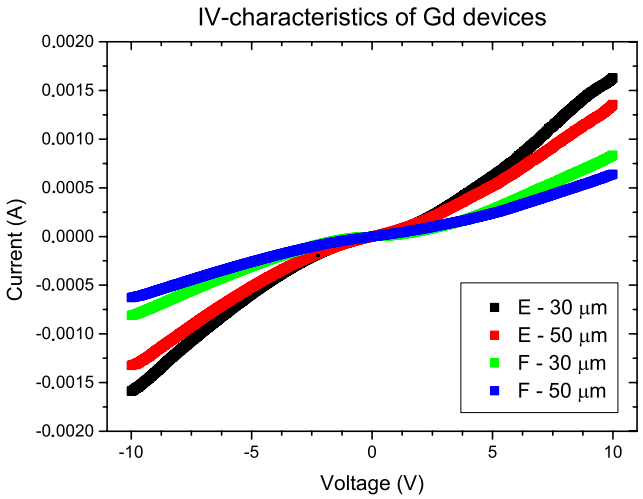

Figure 23: IV-characteristics of Devices E and F - Gd for both 30 μm and 50 μm contact separation at room temperature. Measured in the Parameter Analyzer.

Device F - Gd - 50 μm shows a clear peak around T_C at 50 K. This can be seen in figure 24. Note the very high resistance of the device. Since this device is made using device design II the resistance can be converted to resistivity, which can be seen in figure 25.

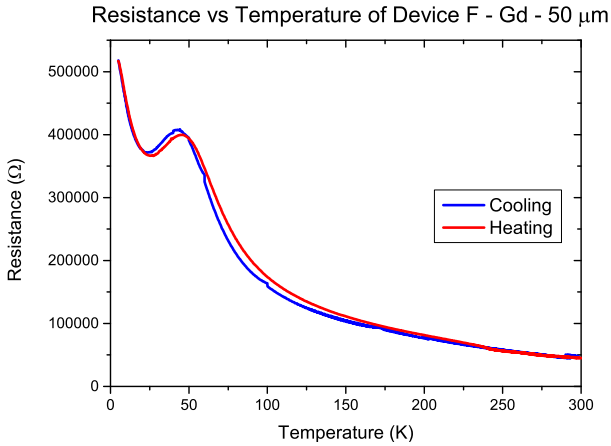

Figure 24: Resistance versus temperature for Device F - Gd - 50 μm.

When studying figure 25 it is clear that the resistivity of the Gd device is a lot higher than the resistivity of the corresponding GdN film. Gd has much lower resistivity than the GdN film in the device and not contribute much to the overall resistivity. This suggests that there are other sources of resistance in the devices.

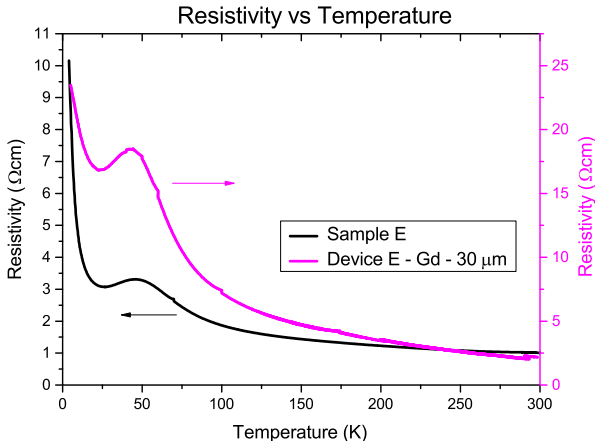

Figure 25: Resistivity versus temperature for Device F - Gd - 50 μm compared to Sample F (a bare GdN film).

The shapes of the curves in figure 25 are not that different but the magnitudes differ greatly. When comparing it to figure 16, in which the resistivities of Sample F and Device F - Au - 30 μm are shown to be very similar, it is obvious that Gd is not ideal for devices demanding overall low resistivity as the Gd contacts increases the resistivity of the device.

The IV-characteristics of Device F - Gd - 50 μm at different temperatures can be seen in figure 26. The curves are all indicative of the Gd making a rectifying junction with the GdN.

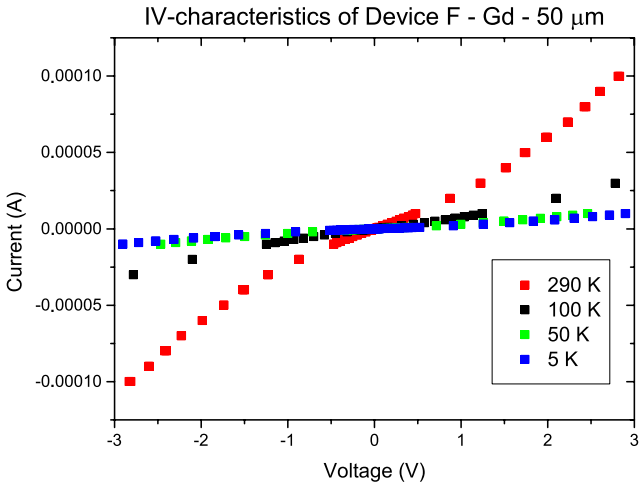

Figure 26: IV-characteristics of Device F - Gd - 50 μm for four different temperatures.

5.6 Titanium-Aluminum contact devices

The Ti/Al contacts were made by first depositing a 15 nm layer of Ti and then a 35 nm layer of Al. All Ti/Al devices were made using device design I.

The Ti/Al devices display the same temperature dependent resistance as the bare GdN films does. This can be seen in figure 27, which is a representative Ti/Al-device. The jumps in the curve are located at the temperatures when the IV-curves where measured, meaning that the jump is probably due to some thermal lag or heating effects in the system.

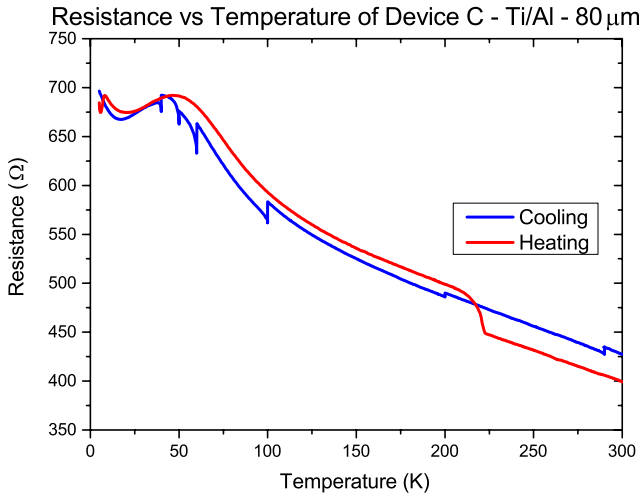

Figure 27: Resistance versus temperature for device C - Ti/Al - 80 µm.

In figure 28 we see that the Ti/Al devices were rectifying at all temperatures for the tested resistivities. The IV-characteristics for the Ti/Al devices are, as well as the Gd devices, displaying back-to-back diode behaviour. Under 100 K the IV-curves change very little with lowering the temperature.

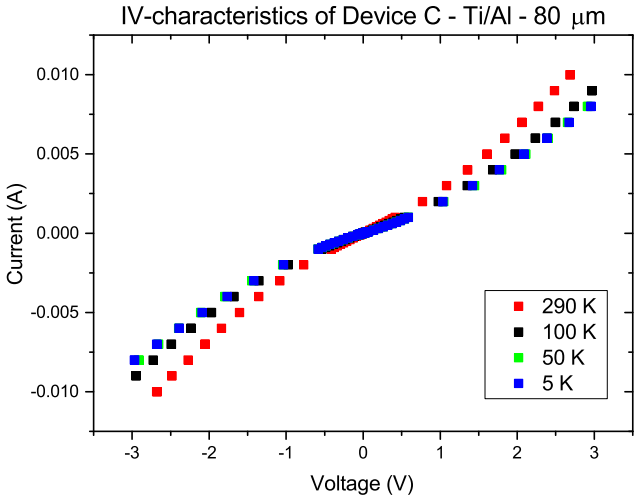

Figure 28: IV-characteristics for device C - Ti/Al - 80 μm.

Figure 29 shows the temperature dependent resistivity of two Ti/Al devices B. It shows that doubling the gap from 40 μm to 80 μm also doubles the resistance. The overall shapes of the curves are very similar as expected. The jump in the 80 μm curve around 225 K is thought to originate from a temperature lag in the system during the heat-up phase of the measurements.

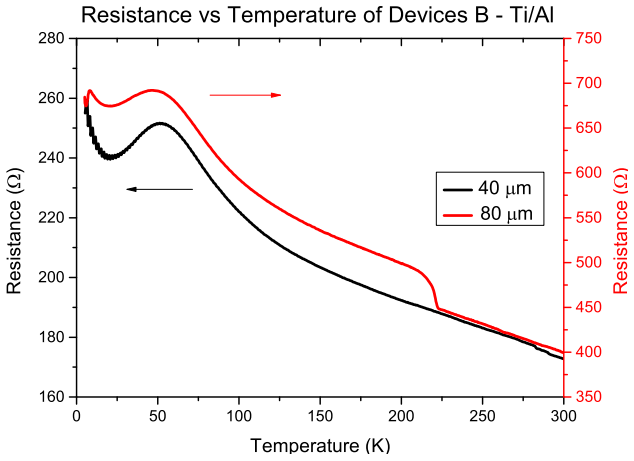

Figure 29: Resistance versus temperature for two devices B - Ti/Al - 40 μm and 80μm.

5.7 Titanium contacts devices

The Ti contacts were 50 nm thick. When the Ti contact devices were taken out of the UHV system after being made they worked fine and were displaying very slightly nonlinear IV-characteristics for large contact separations and almost ohmic for small contact separations. Unfortunately all of the devices oxidised within an hour of leaving the UHV system. This happened for all three different device growths. It was even possible to observe the oxidation process in the microscope as it was taking place.

Doing XRD measurements on the Ti devices does not show any sign of GdN. The part that was GdN is thought to have oxidised despite trying as much as 100 nm of GaN as a capping layer. The GdN formed a powdery amorphous material that fell off during handling as opposed to the polycrystalline GdN which is pretty robust during handling.

In figures 30 and 31 we see the room temperature IV-characteristics of an unoxidised Ti-device and an oxidised one respectively. In figure 31, note the very low current passing through the device and the highly rectifying behaviour.

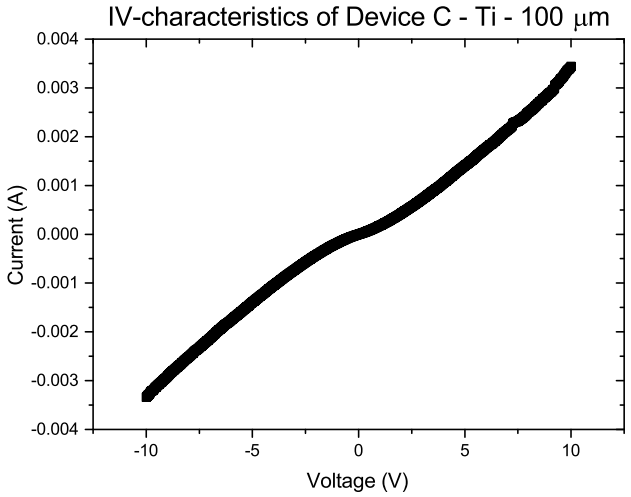

Figure 30: Slightly non-linear IV-characteristics of a Ti device before oxidisation.

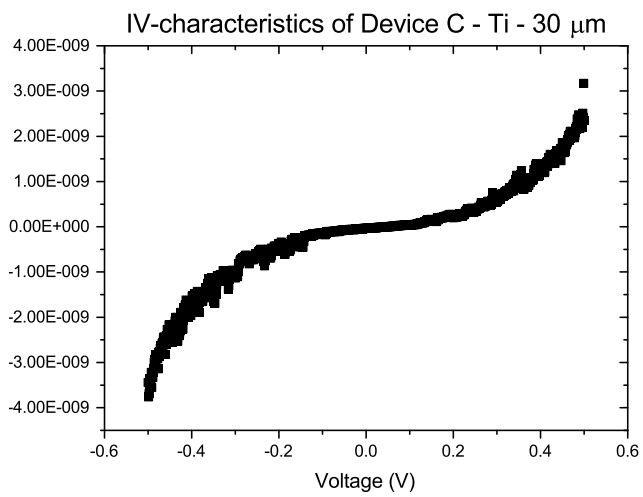

Figure 31: IV-characteristics of a Ti device after oxidisation.

5.8 Ultra-low resistivity GdN Au-devices

Figure 32 shows the temperature dependent resistance of two Device A - Au with different contact separation. Comparing them with their film counterpart, Sample A, in figure 7 we see that the device resistances are clearly dominated by something other than the GdN. However a contribution from the GdN film is clearly visible in the shoulder in resistance around 50 K.

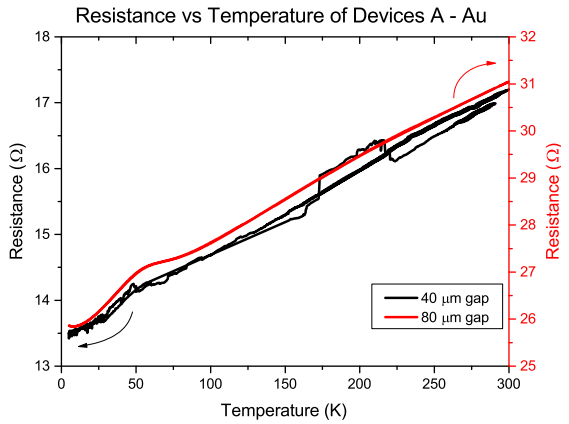

Figure 32: Resistance versus temperature for device A - Au -40 μm and 80 μm.

The reason for the different temperature dependent resistance behaviour of this device is thought to lie in the very low resistivity of the GdN in the device. The very low resistivity of the GdN film makes it possible for other resistances to dominate the total device resistance.

The temperature dependent resistivity for gold is shown in figure 33 where we can see that the behaviour is very similar to the behaviour of the devices A - Au.

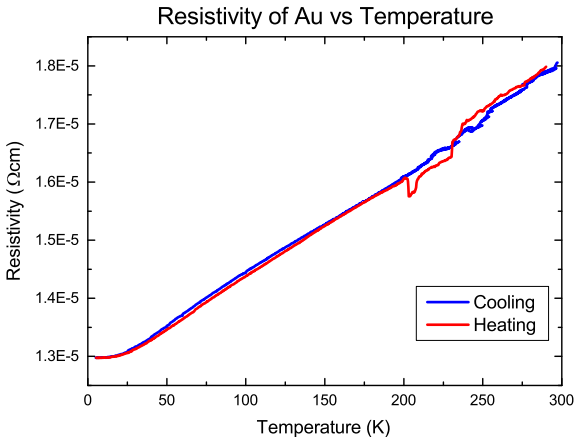

Figure 33: Resistivity versus temperature measured on an empty gold contact.

However, the measured resistivity of the Au means that the Au contact's resistance is about 1 Ω so the Au itself cannot be solely responsible for the behaviour of Device A - Au.

The resistance of the device against the contact separation from measurements in the Parameter Analyzer is plotted in figure 34. From this one can deduce that for zero contact separation there would still be a resistance in the device around 24 Ω. This is thought to be the interface resistance between the Au contact and GdN film. Given that the total device resistance measured in the Parameter Analyzer is between 27 Ω and 40 Ω, the interface resistance of 24 Ω is responsible for a substantial part of the total device resistance. The resistance measured in the cryostat is slightly different since that is a quasi-4-terminal measurement as opposed to a 2-terminal measurement.

Using the resistivity of the GdN film A and the dimensions of the device we can calculate the resistance contribution from the GdN in the device. It is around 1 Ω, meaning that the interface resistance is truly dominating the device.

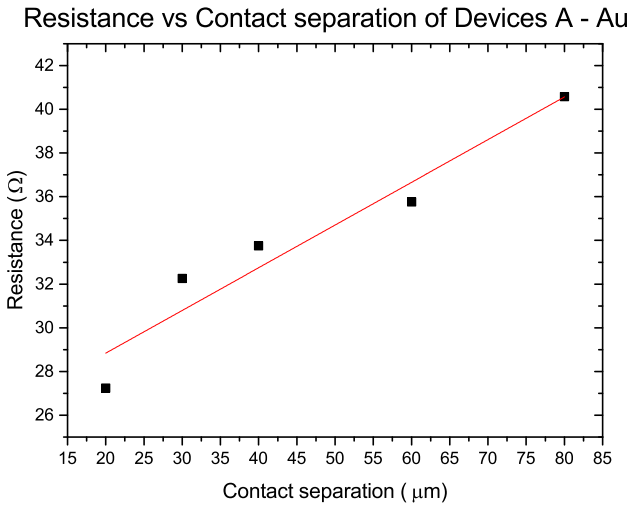

Figure 34: Resistance versus gap size for different contact separations of Devices A - Au. The red line is a linear regression to guide the eyes.

If the junction is ohmic, the total resistance of the device can be seen as a series circuit of all the device component resistances. This can be seen in a sketch in figure 35. The components that contribute are the GdN thin film, the metal contacts, and any interface resistance between the metal contact and GdN arising from the formation of the junction.

Figure 35: A sketch of the proposed resistance relationship in an ohmic device.

In figure 36 we see the IV-characteristics of the Sample A - Au - 40 μm for different temperatures. It displays ohmic behaviour at all measured temperatures strengthening the hypothesis that the interface resistance is the main contributor in the device.

Note however that since the resistance versus temperature graph of this device has a positive temperature coefficient the IV-characteristics at the different temperatures will appear in a different order than the IV-curves of other devices which all have negative temperature coefficients.

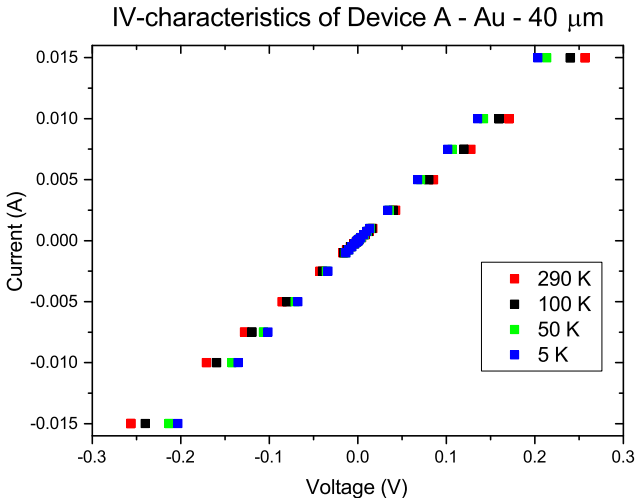

Figure 36: IV-characteristics of Device A - Au - 40 μm at 4 different temperatures.

5.9 Device resistance comparisons

Table 3: GdN film and device data. The I/II in the metal column refers to what device design was used for that particular device. The film resistivities and device resistances are given for 290 K.

Name	**N_2 growth pressure**	**Film resistivity**	**Metal**	**Resistance**
A	$3.2{\cdot}10^{-5}$ mbar	$4.5{\cdot}10^{-4}$ Ωcm	Au (I)	27-40 Ω
B	$2.8{\cdot}10^{-5}$ mbar	0.017 Ωcm	Au (I)	20-50 Ω
			Ag (I)	30-80 Ω
			Ti/Al (I)	100-300 Ω
C	$2.4{\cdot}10^{-5}$ mbar	0.031 Ωcm	Au (I)	20-200 Ω
			Ag (I)	100-200 Ω
			Ti/Al (I)	150-350 Ω
D	$3{\cdot}10^{-5}$ mbar	0.13 Ωcm	Au (I)	70-200 Ω
			Ag (I)	700-900 Ω
			Ti/Al (I)	400-1000 Ω
E	$8{\cdot}10^{-5}$ mbar	0.6 Ωcm	Au (II)	3-5 kΩ
			Ag (I)	0.5-1.4 kΩ
			Gd (II)	7-9 kΩ
F	$5{\cdot}10^{-5}$ mbar	1.0 Ωcm	Au (II)	5-10 kΩ
			Ag (I)	0.7-4 kΩ
			Gd (II)	14-18 kΩ

When studying the contents of Table 3, it is clear that apart from Samples E and F, Au devices work the best as the Au devices has the lowest device resistance for a given GdN film resistivity. In Sample E and F the Ag devices have a lot lower resistance than the Au devices. This could possibly be attributed to the fact that the Au and Gd E- and F-devices have been made with device design II and the Ag E and F-devices are made with device design I. Since device design II requires the whole device to soak in acetone to allow the GdN outside of the photolithography patter to lift-off it is possible that the GdN films have oxidised slightly by being in acetone for a few minutes thereby increasing the total device resistance. This hypothesis is supported by data presented earlier. Gd and Ti/Al devices have the highest device resistances relative to the Au devices and are also the devices which are rectifying.

6 Discussion

Looking at the IV-curves of devices made with Ti/Al they are clearly non-linear, but not hugely so. This would make it seem that the SBH for these devices is not very high. Unfortunately the SHB was not able to be determined due to the devices behaving too linearly in the studied voltage range. Higher voltages were not possible to use in the experimental setups used in this thesis.

Devices made with Gd seem to have a more rectifying behaviour than Ti/Al devices, as their IV-characteristics are more non-linear. This can be seen as a bit odd, given that Gd has a lower work function than both Ti and Al. The most resistive device with Ti/Al contacts has been made with a GdN film resistivity of 0.13 Ωcm at room temperature and the lowest film resistivity in a Gd device has a resistivity of 0.6 Ωcm. This means that the Gd devices are more resistive, with fewer charge carriers in the GdN films. A higher voltage then has to be applied to achieve the same current through the device. Rectifying devices are interesting for use in for example field effect transistors.

Both Au and Ag contact devices display ohmic IV-characteristics. However devices with Au contacts have a lower overall device resistance, suggesting they would be better as contacts in devices where small currents and voltages are used. Ag devices, having a higher resistance, could be used in device where one is interested in limiting the current as well as utilising the behaviour of GdN.

It was thought that the difference in sharpness of the boundaries in the devices from the different device designs could have an effect on the device performances since it would effect the contact area between the GdN and metal and as such the amount of surface states and of metal diffusion into the GdN. Looking at the AFM results it would appear that most device have quite similar boundary sharpnesses, independent of their device design. It would be natural to think that the device made with design I using the shadow mask would have a less well defined contact boundary since they have an uneven metal influx over the area of the contact due to the substrate holder in the Evaporator not being able to rotate to minimise the influx of metal under the shadow mask. This doesn't seem to be the case for Au and Ag devices. The Ti/Al contact exhibits this behaviour showing a more gently sloping boundary, probably due to the contact being a bilayer and the two layers being deposited with a very slight lateral offset.

Of the two different device design made, device structure II offers the most interesting setup for determining the behaviour of the junction between the metal and GdN. In device structure II there are four pre-deposited metal contacts which allows the resistivity of the device to be measured while removing the resistance created when making electrical contact to the device. This ensures that the resulting measured resistance and resistivity is only that of the device. It also makes it possible to average the resistance measured over two different gaps in the same

device, making slight abnormalities in a device of structure II less of a problem than in device structure I. Device structure II does unfortunately involve soaking the entire device in acetone as it is made using photolithography. This could possibly explain why Au and Gd devices E and F (made in structure II) have higher resistances than Ag devices E and F (made in structure I) which is opposite to what one would expect from the previous devices where Au device are the least resistive. This could possibly be circumvented by using photolithography to make the metal contacts but a shadow mask when depositing the GdN and GaN.

It would be interesting to determine the SBHs of these devices, but this was not done due to the time constraints of the thesis work. It is especially interesting since the opposite to predicted behaviour is observed, the highest work function metals (Au and Ag) make ohmic contacts while the lowest work function metals (Ti, Al and Gd) make Schottky contacts. This can probably be attributed to a combination of surface oxidation of the metals, different diffusivities of the metals in GdN, surface states, quality of the contact and GdN films, and other things. Surface oxides are suspected to be present in the Ti, Al, and Gd contacts in varying degrees. The oxides of these metals provides another, often insulating, component to the junction. This could explain why the Gd and Ti/Al devices show rectifying behaviour despite having lower work functions than Au and Ag as Gd, Ti, and Al quickly form an oxide layer on the surface when in contact with air. This could possibly be remedied by annealing or sputtering the metal contacts before depositing GdN.

No change from ohmic to rectifying, or the other way around, was found in the IV-characteristics of any device when going below the Curie temperature. When comparing the temperature dependent resistance graphs for a device and a bare GdN film no major differences can be seen. The overall shape, the location of the Curie temperature, and magnitude of the peak at the Curie temperature are all very similar for devices and their corresponding GdN film. This indicates that the metals are not influencing the magnetic behaviour of the GdN film.

All devices show some interface resistance, but it is most prominent in the ultra-low resistivity GdN Au devices. The interface resistance could arise due surface states of the GdN and Au, changing the electronic structure locally. Another possibility is diffusion of atoms between the GdN and the Au, creating other compounds at the interface with have higher resistances than either the GdN and Au. It is also possible that the polycrystalline nature of the GdN film contributes, as the size of the crystallites are on the order of the contact separation distance, and more surface states than for an epitaxial film might be present.

7 Conclusion

Devices made of metal-GdN-metal junctions have been designed and fabricated. The temperature dependent resistivity for their corresponding films has been measured using a van der Pauw setup as well as the films' crystalline quality using XRD. The surface roughness of the GaN capping layer was measured to be 1.5 nm using an AFM.

The devices were characterised by temperature dependent resistance measurement as well as their IV-characteristics at different temperatures from 300 K to 5 K. Devices with Au and Ag contact devices were found to be ohmic at all temperatures whereas Gd and Ti/Al contact devices were found to be rectifying at all temperatures. Ti devices oxidised within an hour of leaving the UHV system. Most devices were found to have well defined sharp step boundaries between the different device components when studying them in the AFM.

Devices with Au contacts had a resistivity very similar in behaviour and magnitude to a bare GdN film. Gd devices showed a similar behaviour to the bare GdN film but with about twice the resistivity. Devices with Ag and Ti/Al contacts show similar temperature dependent resistance as the bare GdN does, but due only having 2 metal contacts their resistance could not be converted to resistivity and as such it can't be compared directly to the bare GdN.

8 Outlook

This thesis deals with the study of the electrical properties of metal-GdN-metal junctions at different temperatures to aid the design of future GdN-based spintronic devices.

Using the knowledge acquired from this work it is possible to select a contact metal that gives either a ohmic junction to GdN or a rectifying one. It is also possible to tune the total resistance of the device as both Au and Ag give ohmic devices but with different resistance despite being made with a GdN film of the same resistivity. This allows for more specialised device designs depending on the desired functionality of the device. It also allows for device optimisation by choice of contact metals.

Furthering the work that has been done in this thesis could be to determine the SBH for the different devices, investigate what effect annealing the contacts might have, sputter cleaning to contacts before GdN deposition to ensure that there are no oxides and if the different metals work the the same way when used as contacts to epitaxial GdN films.

It would also be interesting to study how the IV-characteristics of the devices look under magnetic fields to investigate is there is a magnetic coupling between the GdN and the metal contacts. This would be useful information for many proposed device implementations, either to avoid coupling or to use the metal to strengthen certain aspects of the device behaviour.

9 Acknowledgements

The author would like to acknowledge the assistance of the following:
Franck Natali, supervisor at Victoria University of Wellington (VUW)
Jonas Johansson, supervisor at Lund University
Natalie Plank, lecturer at VUW, and Hanna Zheng, PhD student at VUW, for teaching photolithography
Harry Warring, PhD student at VUW, for assistance on countless experimental issues
Jay Chan, PhD student at VUW, for assistance with doing X-ray reflectivity and for help with experimental issues
Leo Browning, laboratory assistant at VUW, for assistance with AFM imaging.
Joe Trodahl, Ben Ruck, and the rest of the Spintronics group for helpful comments and discussions.

10 References

1. Natali, F., Ruck, B. J., Plank, N. O. V., Trodahl, H. J., Granville, S., Meyer, C. & Lambrecht, W. R. L. Rare-earth mononitrides. *Prog. Mater. Sci.* **58,** 1316–1360 (2013).
2. Han, S. Y., Hite, J., Thaler, G. T., Frazier, R. M., Abernathy, C. R., Pearton, S. J., Choi, H. K., Lee, W. O., Park, Y. D., Zavada, J. M. & Gwilliam, R. Effect of Gd implantation on the structural and magnetic properties of GaN and AlN. *Appl. Phys. Lett.* **88,** 042102 (2006).
3. Dhar, S., Brandt, O., Ramsteiner, M., Sapega, V. F. & Ploog, K. H. Colossal magnetic moment of Gd in GaN. *Phys. Rev. Lett.* **94,** 037205 (2005).
4. Schwarz, B., Mattern, N., Luo, Q. & Eckert, J. Magnetic properties and magnetocaloric effect of rapidly quenched Gd-Co-Fe-Al alloys. *J. Magn. Magn. Mater.* **324,** 1581–1587 (2012).
5. Granville, S., Ruck, B., Budde, F., Koo, A., Pringle, D., Kuchler, F., Preston, A., Housden, D., Lund, N., Bittar, A., Williams, G. & Trodahl, H. Semiconducting ground state of GdN thin films. *Phys. Rev. B* **73,** 235335 (2006).
6. Warring, H., Ruck, B. J., Trodahl, H. J. & Natali, F. Electric field and photo-excited control of the carrier concentration in GdN. *Appl. Phys. Lett.* **102,** 132409 (2013).
7. Natali, F., Plank, N. O. V., Galipaud, J., Ruck, B. J., Trodahl, H. J., Semond, F., Sorieul, S. & Hirsch, L. Epitaxial growth of GdN on silicon substrate using an AlN buffer layer. *J. Cryst. Growth* **312,** 3583–3587 (2010).
8. Aerts, C. M., Strange, P., Horne, M., Temmerman, W. M., Szotek, Z. & Svane, A. Half-metallic to insulating behavior of rare-earth nitrides. *Phys. Rev. B* **69,** 045115 (2004).

9. Lee, C.-M., Warring, H., Vézian, S., Damilano, B., Granville, S., Al Khalfioui, M., Cordier, Y., Trodahl, H. J., Ruck, B. J. & Natali, F. Highly resistive epitaxial Mg-doped GdN thin films. *Appl. Phys. Lett.* **106,** 022401 (2015).
10. Duan, C.-G., Sabirianov, R. F., Mei, W. N., Dowben, P. A., Jaswal, S. S. & Tsymbal, E. Y. Electronic, magnetic and transport properties of rare-earth monopnictides. *J. Phys. Condens. Matter* **19,** 315220 (2007).
11. Preston, A. R. H. *Electronic Structure of the Rare-Earth Nitrides* Doctor of Philosophy (Victoria University of Wellington, 2010).
12. Senapati, K., Blamire, M. G. & Barber, Z. H. Spin-filter Josephson junctions. *Nat. Mater.* **10,** 849–52 (2011).
13. Senapati, K., Blamire, M. G. & Barber, Z. H. Suppression of magnetic coupling in superconducting GdN-NbN-GdN trilayers. *Appl. Phys. Lett.* **103,** 132406 (2013).
14. Krishnamoorthy, S., Kent, T. F., Yang, J., Park, P. S., Myers, R. C. & Rajan, S. GdN nanoisland-based GaN tunnel junctions. *Nano Lett.* **13,** 2570–2575 (2013).
15. Sivkov, I. N., Brovko, O. O. & Stepanyuk, V. S. Spin-polarized transport properties of GdN nanocontacts. *Phys. Rev. B* **89,** 195419 (2014).
16. Kandala, A., Richardella, A., Rench, D. W., Zhang, D. M., Flanagan, T. C. & Samarth, N. Growth and characterization of hybrid insulating ferromagnet-topological insulator heterostructure devices. *Appl. Phys. Lett.* **103,** 202409 (2013).
17. Warring, H., Trodahl, H. J., Plank, N. O. V., Natali, F. & Ruck, B. J. *Submitted to Phys. Rev. Appl.* (2015).
18. Žutić, I., Fabian, J. & Sarma, S. D. Spintronics: Fundamentals and applications. *Rev. Mod. Phys.* **76,** 323–410 (2004).
19. Wolf, S. A., Awschalom, D. D., Buhrman, R. A., Daughton, J. M., von Molnár, S., Roukes, M. L., Chtchelkanova, A. Y. & Treger, D. M. Spintronics: a spin-based electronics vision for the future. *Science* **294,** 1488–1495 (2001).
20. Awschalom, D. D. & Kikkawa, J. M. Electron spin and optical coherence in semiconductors. *Phys. Today* **52,** 33–38 (1999).
21. Murmu, P. P., Kennedy, J., Williams, G. V. M., Ruck, B. J., Granville, S. & Chong, S. V. Observation of magnetism, low resistivity, and magnetoresistance in the near-surface region of Gd implanted ZnO. *Appl. Phys. Lett.* **101,** 082408 (2012).
22. Chen, Z. T., Wang, L., Yang, X. L., Wang, C. D. & Zhang, G. Y. Mechanism of ultra-high Mn concentration in epitaxially grown wurtzite $Ga_{1-x}Mn_xN$. *Appl. Phys. Lett.* **97,** 222108 (2010).
23. Navarro-Quezada, A., Stefanowicz, W., Li, T., Faina, B., Rovezzi, M., Lechner, R. T., Devillers, T., D'Acapito, F., Bauer, G., Sawicki, M., Dietl, T. & Bonanni, A. Embedded magnetic phases in (Ga,Fe)N: Key role of growth temperature. *Phys. Rev. B* **81,** 205206 (2010).
24. Dobrowolska, M., Tivakornsasithorn, K., Liu, X., Furdyna, J. K., Berciu, M., Yu, K. M. & Walukiewicz, W. Controlling the Curie temperature in (Ga,Mn)As through location of the Fermi level within the impurity band. *Nat. Mater.* **11,** 444–449 (2012).

25. Larson, P., Lambrecht, W. R. L., Chantis, A. & Van Schilfgaarde, M. Electronic structure of rare-earth nitrides using the LSDA+U approach: Importance of allowing 4f orbitals to break the cubic crystal symmetry. *Phys. Rev. B* **75,** 045114 (2007).
26. Plank, N. O. V., Natali, F., Galipaud, J., Richter, J. H., Simpson, M., Trodahl, H. J. & Ruck, B. J. Enhanced Curie temperature in N-deficient GdN. *Appl. Phys. Lett.* **98,** 112503 (2011).
27. Ruck, B., Natali, F., Plank, N. O. V., Do Le, B., Azeem, M., Alfheid, M., Meyer, C. & Trodahl, H. The influence of nitrogen vacancies on the magnetic behaviour of rare-earth nitrides. *Physica B* **407,** 2954–2956 (2012).
28. Li, D. X., Haga, Y., Shida, H., Suzuki, T., Kwon, Y. S. & Kido, G. Magnetic properties of stoichiometric Gd monopnictides. *J. Phys. Condens. Matter* **9,** 10777–10788 (1999).
29. Duan, C.-G., Sabiryanov, R. F., Mei, W. N., Dowben, P. A., Jaswal, S. S. & Tsymbal, E. Y. Magnetic ordering in Gd monopnictides: Indirect exchange versus superexchange interaction. *Appl. Phys. Lett.* **88,** 182505 (2006).
30. Senapati, K., Fix, T., Vickers, M. E., Blamire, M. G. & Barber, Z. H. Structural evolution and competing magnetic orders in polycrystalline GdN films. *Phys. Rev. B* **83,** 014403 (2011).
31. Trodahl, H. J., Preston, A. R. H., Zhong, J., Ruck, B. J., Strickland, N. M., Mitra, C. & Lambrecht, W. R. L. Ferromagnetic redshift of the optical gap in GdN. *Phys. Rev. B* **76,** 085211 (2007).
32. Yoshitomi, H., Kitayama, S., Kita, T., Wada, O., Fujisawa, M., Ohta, H. & Sakurai, T. Optical and magnetic properties in epitaxial GdN thin films. *Phys. Rev. B* **83,** 155202 (2011).
33. Natali, F., Vézian, S., Granville, S., Damilano, B., Trodahl, H. J., Anton, E. M., Warring, H., Semond, F., Cordier, Y., Chong, S. V. & Ruck, B. J. Molecular beam epitaxy of ferromagnetic epitaxial GdN thin films. *J. Cryst. Growth* **404,** 146–151 (2014).
34. Khazen, K., von Bardeleben, H., Cantin, J., Bittar, A., Granville, S., Trodahl, H. & Ruck, B. Ferromagnetic resonance study of GdN thin films with bulk and extended lattice constants. *Phys. Rev. B* **74,** 245330 (2006).
35. Mitra, C. & Lambrecht, W. R. L. Magnetic exchange interactions in the gadolinium pnictides from first principles. *Phys. Rev. B* **78,** 134421 (2008).
36. Sharma, A. & Nolting, W. Additional carrier-mediated ferromagnetism in GdN. *Phys. Rev. B* **81,** 125303 (2010).
37. Leuenberger, F., Parge, A., Felsch, W., Fauth, K. & Hessler, M. GdN thin films: Bulk and local electronic and magnetic properties. *Phys. Rev. B* **72,** 014427 (2005).
38. Natali, F., Ruck, B., Trodahl, H., Binh, D., Vezian, S., Damilano, B., Cordier, Y., Semond, F. & Meyer, C. Role of magnetic polarons in ferromagnetic GdN. *Phys. Rev. B* **87,** 035202 (2013).
39. Gerlach, J. W., Mennig, J. & Rauschenbach, B. Epitaxial gadolinium nitride thin films. *Appl. Phys. Lett.* **90,** 24–27 (2007).

40. Scarpulla, M. A., Gallinat, C. S., Mack, S., Speck, J. S. & Gossard, A. C. GdN (111) heteroepitaxy on GaN (0001) by N2 plasma and NH3 molecular beam epitaxy. *J. Cryst. Growth* **311,** 1239–1244 (2009).
41. Schroder, D. K. *Semiconductor Material and Device Characterization* 3rd ed. **4,** 1–779 (John Wiley & Sons, Inc, 2005).
42. Chiquito, A. J., Amorim, C. A., Berengue, O. M., Araujo, L. S., Bernardo, E. P. & Leite, E. R. Back-to-back Schottky diodes: the generalization of the diode theory in analysis and extraction of electrical parameters of nanodevices. *J. Phys. Condens. Matter* **24,** 225303 (2012).
43. Foresi, J. S. & Moustakas, T. D. Metal contacts to gallium nitride. *Appl. Phys. Lett.* **62,** 2859–2861 (1993).
44. Lee, C.-T. & Kao, H.-W. Long-term thermal stability of Ti/Al/Pt/Au Ohmic contacts to n-type GaN. *Appl. Phys. Lett.* **76,** 2364–2366 (2000).
45. Pal, S. & Sugino, T. Fabrication and characterization of metal/GaN contacts. *Appl. Surf. Sci.* **161,** 263–267 (2000).
46. Fan, Z., Mohammad, S. N., Kim, W., Aktas, Ö., Botchkarev, A. E. & Morkoç, H. Very low resistance multilayer Ohmic contact to n-GaN. *Appl. Phys. Lett.* **68,** 1672–1674 (1996).
47. Zhao, W., Mohammed, F. M. & Adesida, I. Application of the Ag-based ohmic contact to the realization of thermally-stable InAlAs/InGaAs/InP high electron mobility transistors. *Japanese J. Appl. Physics, Part 1 Regul. Pap. Short Notes Rev. Pap.* **45,** 7632–7636 (2006).
48. Dumas, D. C. S., Gallacher, K., Millar, R., Maclaren, I., Myronov, M., Leadley, D. R. & Paul, D. J. Silver antimony Ohmic contacts to moderately doped n-type germanium. *Appl. Phys. Lett.* **104,** 162101 (2014).
49. Zutić, I. Spintronics: Gadolinium makes good spin contacts. *Nat. Mater.* **5,** 771–772 (2006).
50. Skriver, H. L. & Rosengaard, N. M. Surface-Energy and Work Function of Elemental Metals. *Phys. Rev. B* **46,** 7157–7168 (1992).
51. Eastman, D. E. Photoelectric work functions of transition, rare-earth, and noble metals. *Phys. Rev. B* **2,** 1–2 (1970).
52. Farrow, R. F. in *Molecular Beam Epitaxy: Applications to Key Materials* chap. 1 (Elsevier, 1995).
53. Pohl, U. W. *Epitaxy of Semiconductors* (Springer, BERLIN, 2012).
54. Green, M. A. & Gunn, M. W. The evaluation of geometrical effects in four point probe measurements. *Solid. State. Electron.* **14,** 1167–1177 (1971).
55. Green, M. A. & Gunn, M. W. Four point probe Hall effect and resistivity measurements upon semiconductors. *Solid. State. Electron.* **15,** 577–585 (1972).
56. Logan, M. A. Sheet resistivity measurements on rectangular surfaces-general solution for four point probe conversion factors. *Bell Syst. Tech. J.* **46,** 2277–2322 (1967).

57. Perloff, D. S. Four-point sheet resistance correction factors for thin rectangular samples. *Solid. State. Electron.* **20,** 681–687 (1977).
58. Martin-Palma, R. J. & Lakhtakia, A. in *Nanotechnology - A Crash Course* chap. 4 (SPIE Publications, 2010).